CD4 + T cells require Ikaros to inhibit their differentiation towards a pathogenic cell fate

Chiara Bernardi, Gaëtan Maurer, Tao Ye, Patricia Marchal, Bernard Jost, Manuela Wissler, Ulrich Maurer, Philippe Kastner, Susan Chan, Céline Charvet

PNAS
www.pnas.org

Main Manuscript for

CD4+ T cells require Ikaros to inhibit their differentiation towards a pathogenic cell fate

Chiara Bernardi[†,‡,§,¶], Gaëtan Maurer[†,‡,§,¶], Tao Ye[†,‡,§,¶,††], Patricia Marchal[†,‡,§,¶], Bernard Jost[†,‡,§,¶,††], Manuela Wissler[‡‡], Ulrich Maurer[‡‡,§§,¶¶], Philippe Kastner[†,‡,§,¶,##,*], Susan Chan[†,‡,§,¶,*] and Céline Charvet[†,‡,§,¶,*]

***Correspondence:**
Céline Charvet (charvetc@igbmc.fr)
Philippe Kastner and Susan Chan (scpk@igbmc.fr)
IGBMC, 1 rue Laurent Fries, BP 10142, 67404 Illkirch CEDEX, France

ORCID ID:
Bernardi Chiara (0000-0001-5118-5402), Maurer Gaëtan (0000-0003-2869-0595), Ye Tao (0000-0002-3394-2083), Marchal Patricia (0000-0001-6505-4956), Jost Bernard (0000-0002-3722-3457), Maurer Ulrich (0000-0002-2504-1517), Kastner Philippe (0000-0002-9113-8878), Chan Susan (0000-0001-5493-5985) and Charvet Céline (0000-0003-1828-3400)

Author contribution:
CB, GM, PK, SC and CC designed the study, performed experiments, analyzed data, and wrote the manuscript. PM and MW performed experiments. BJ performed high throughput sequencing experiments. UM performed experiments and contributed essential reagents. TY analyzed data.

Competing Interest Statement: The authors have no conflicts of interest.

Classification: BIOLOGICAL SCIENCES (Immunology and Inflammation)

Running title: Ikaros limits pathogenic T cell development

Keywords: Ikaros, Th17, IL-17, GM-CSF, pro-inflammatory cytokines, pathogenicity

This PDF file includes: Main text and Figures 1 to 7

[†] Institut de Génétique et de Biologie Moléculaire et Cellulaire (IGBMC), Illkirch, France
[‡] Centre National de la Recherche Scientifique (CNRS), UMR7104, Illkirch, France
[§] Institut National de la Santé et de la Recherche Médicale (INSERM), U1258, Illkirch, France
[¶] Université de Strasbourg, Strasbourg, France
[††] Plateforme GenomEast, Infrastructure France Génomique, Illkirch, France
[‡‡] Institute of Molecular Medicine and Cell Research, Faculty of Medicine, Albert- Ludwigs-University of Freiburg, Freiburg, Germany
[§§] Spemann Graduate School of Biology and Medicine (SGBM), Albert-Ludwigs-University of Freiburg, Freiburg, Germany
[¶¶] BIOSS, Centre for Biological Signaling Studies, Hebelstrasse 2, 79104 Freiburg, Germany
[##] Faculté de Médecine, Université de Strasbourg, Strasbourg, France

ABSTRACT

The production of pro-inflammatory cytokines, particularly GM-CSF, by pathogenic $CD4^+$ T cells is central for mediating tissue injury in inflammatory and autoimmune diseases. However, the factors regulating the T cell pathogenic gene expression program remain unclear. Here, we investigated how the Ikaros transcription factor regulates the global gene expression and chromatin accessibility changes in murine T cells during Th17 polarization and after activation via the TCR and CD28. We found that, in both conditions, Ikaros represses the expression of genes from the pathogenic signature, particularly *Csf2,* which encodes GM-CSF. We show that, in TCR/CD28-activated T cells, Ikaros binds a critical enhancer downstream of *Csf2*, and is required to regulate chromatin accessibility at multiple regions across this locus. Genome wide, Ikaros binding is associated with more compact chromatin, notably at multiple sites containing NFκB or STAT5 target motifs, and STAT5 or NFκB inhibition prevents GM-CSF production in Ikaros-deficient cells. Importantly, Ikaros also limits GM-CSF production in TCR/CD28-activated human T cells. Our data thus highlight a critical conserved transcriptional mechanism that antagonizes GM-CSF expression in T cells.

SIGNIFICANCE STATEMENT

The production of pro-inflammatory cytokines, particularly GM-CSF, by $CD4^+$ T cells is a key process for amplifying immune responses, but can also lead to harmful tissue damage in pathologies like multiple sclerosis, and Covid-19. Correctly controlling the expression of pro-inflammatory cytokines is thus of major interest. However, the pathogenic signature of $CD4^+$ T cells relies on a transcriptional program that is thus far poorly understood. Here, we identified the transcription factor Ikaros as an essential transcriptional repressor of pro-inflammatory cytokine gene expression. Our work identifies a critical molecular pathway regulating the pathogenic program of $CD4^+$ T cells, and brings new perspectives for potential therapies of autoimmune and inflammatory diseases.

INTRODUCTION

Upon antigen recognition and depending on the cytokine context, naive $CD4^+$ T cells polarize into different effector populations. $CD4^+$ T cells become IL-17-secreting Th17 cells in the presence of IL-6 and TGFβ1, and the induction of the RORγt transcription factor is central to this process *(1, 2)*. IL-17^+ T cells are important for clearing fungi and extracellular bacterial infections, and have been implicated in gut homeostasis. They are often called conventional (c), or "non-pathogenic," Th17 cells because they do not induce tissue inflammation *(3)*, and possess immunoregulatory functions through IL-10 secretion *(4)*. On the other hand, $CD4^+$ T cells become "pathogenic" (p)Th17 cells with the addition of IL-23, or in the presence of IL-23, IL-1β and IL-6 *(5, 6)*. pTh17 cells promote autoimmunity and have been reported to induce experimental autoimmune encephalomyelitis (EAE), the murine model for multiple sclerosis, via their production of pro-inflammatory cytokines *(5-8)*. $CD4^+$ T cells can also differentiate into pathogenic Th1 and Th-GM cells which themselves contribute to autoimmune disease progression *(9-11)*. Thus, naive $CD4^+$ T cells can polarize into multiple types of pathogenic effector cells with unique phenotypes. All of them are characterized by the high production of the pro-inflammatory cytokine, granulocyte-macrophage-colony stimulating factor (GM-CSF).

Indeed, GM-CSF production is tightly associated with T cell pathogenicity. Local GM-CSF production by T cells is closely linked to tissue inflammation in neuropathological disorders like multiple sclerosis *(12, 13)*. High GM-CSF production has also been observed in patients with Coronavirus disease 2019 (Covid-19) *(14-16)*, suggesting a potential target for treatment. How GM-CSF expression is regulated is only partially understood, but this knowledge is of considerable importance.

GM-CSF is encoded by the *Csf2* gene, which requires TCR and CD28 pathways to be expressed in T cells *(17)*, as well as IL-23 and IL-7 signaling in some cases *(6-8, 10)*. Transcription of the *Csf2* gene is controlled by the *Csf2* promoter and two enhancers, one located ~1.5 kb upstream and a conserved non-coding sequence (CNSa) ~34 kb downstream of the transcriptional start site *(18-20)*. The promoter contains binding sequences for the transcription factors NFAT, NFκB, AP-1 and Brg1, and is sensitive to changes in chromatin accessibility *(21-28)*. *Csf2* promoter activity is potentiated upon NFAT and AP-1 binding to the upstream enhancer, and NFκB and Brg1 binding to the CNSa region *(19, 20)*. In addition, STAT5 and the Foxo3-Eomes axis have been described to be important for GM-CSF production in Th-GM and Th1 cells, respectively, and for influencing the pathogenic potential of these cells *(9, 10, 29)*. Most of the factors identified so far have been transcriptional activators. However, given the centrality of this cytokine in inflammation and

autoimmunity, we hypothesized that negative regulators of *Csf2* expression must be equally important for the regulation of this gene.

Here, we characterize the role of the Ikaros transcription factor in regulating GM-CSF production during T cell activation and Th17 polarization. We show that Ikaros is a direct repressor of *Csf2* mRNA expression, and that Ikaros is required to limit the pathogenic gene expression program in activated T cells.

RESULTS

Ikaros represses a pathogenic gene expression program in CD4$^+$ T cells

Up to now, the role of Ikaros in Th17 cell differentiation and IL-17 production has been unclear. IL-17 expression by cTh17-polarized cells is severely blunted in germline Ikaros null mice *(30)*, but seems inconsistently affected in animals where Ikaros is deleted in peripheral T cells *(31)*. In contrast, IL-17 production is enhanced in Th17 cells from mice with a targeted deletion of the fourth DNA-binding zinc finger (ZnF4) of Ikaros *(32)*. To clarify the role of Ikaros in Th17 polarization, we studied Ik$^{f/f}$ CD4-Cre$^+$ (TKO) mice where *Ikzf1* is selectively deleted in T cells (**SI appendix, Fig. S1A**) *(33)*. Purified naive CD4$^+$CD25$^-$ CD44$^{lo/-}$TCR$\gamma\delta^-$NK1.1$^-$ T (TN) cells from TKO and WT (Ik$^{f/f}$ CD4-Cre$^-$) lymph nodes were stimulated with anti-CD3 and anti-CD28 antibodies (Ab) alone ("Th0 conditions"), or in the presence of IL-6 and TGFβ1 ("Th17 conditions"). Cytoplasmic IL-17 production was analyzed after 3 days by flow cytometry (**Fig. 1A**). In these cultures, the majority of WT cells were induced to make IL-17 under Th17 compared with Th0 conditions (67% vs. 1.2%, respectively), as expected, while TKO cells made little to no IL-17 in either condition. Therefore, naive CD4$^+$ T cells cannot produce IL-17 in response to Th17 cell polarization without Ikaros.

To understand the Th17 response in the absence of Ikaros, we evaluated the gene expression profiles of WT and TKO naive CD4$^+$ T cells, cultured in Th17 conditions (and in the presence of anti-IFNγ and anti-IL-4 neutralizing Abs to block indirect effects), over time (days 0, 1 and 2), by microarray analysis. These experiments revealed that WT and TKO cells responded similarly in general to Th17 conditions, as the majority of the up- (>3000) and downregulated (>1500) genes overlapped between genotypes at days 1 and 2 (FC>1.42) (**SI appendix, Fig. S1, B and C**). Still, there were clear differences. Principal component analysis (PCA) revealed that WT and TKO cells were distinct at every timepoint (**Fig. 1B**). Among the upregulated genes, Th17-associated genes were less upregulated in TKO cells with time, like *Il17a* and *-f*, *Il21* and *Rorc* (clusters 11, 12) (**SI appendix, Fig. S1B**). *Il17a* and *Rorc* mRNA levels were confirmed by qRT-PCR (**SI appendix, Fig. S1D**). Cell cycle-related genes were also less induced in TKO cells (cluster 18) (**SI appendix, Fig. S1, B and E**).

Interestingly, three clusters of genes were ectopically expressed in Th17 conditions in the absence of Ikaros (**Fig. 1C**). Cluster 1 contained genes that were constitutively expressed in naive TKO CD4$^+$ T cells and remained expressed over time; it included genes encoding Helios (*Ikzf2*) and NFATc1 (*Nfatc1*). Clusters 2 and 3 contained genes that were similarly expressed in WT and TKO cells at day 0, but were strongly induced in the mutant

cells at day 1 or 2; they included genes encoding pro-inflammatory cytokines (eg. *Ifng*, *Csf2*, *Il1a*, *Il3*, *Il13*, *Il22*, *Ccl3*, *Ccl4*) or their receptors (eg. *Il23r*, *Cxcr3*) (**Fig. 1, C-E**). On the other hand, the anti-inflammatory cytokine gene *Il10* was induced but less upregulated in TKO cells (cluster 12) (**SI appendix Fig. S1B and Fig. 1D**).

Since pro-inflammatory cytokines are characteristic of pathogenic Th17 cells, we performed a gene set enrichment analysis (GSEA) with the most differentially expressed genes between TKO and WT samples, and compared them with genes highly expressed in pTh17 or cTh17 cells *(6)*. This showed a strong and direct correlation between TKO T cells and pTh17, but not cTh17, cells (**Fig. 1F and SI appendix, Fig. S2A**), suggesting that TKO $CD4^+$ T cells resemble pTh17 cells after stimulation. We also compared TKO cells with the recently described Th-GM cells *(10)*, and Th17 cells from the central nervous system of mice with EAE *(34)* and found a strong correlation between the genes differentially expressed in TKO and those expressed in these T cell populations (**SI appendix, Figs. S2B and S2C**).

Collectively, these results indicated that activated $CD4^+$ T cells cannot produce IL-17 and enter a pro-inflammatory gene program in the absence of Ikaros.

Ikaros is required in $CD4^+$ T cells to coordinate cytokine responses

To determine if Ikaros loss during thymocyte differentiation impacts the state of naive $CD4^+$ T cells to lead to the abnormal response, we acutely deleted the *Ikzf1* alleles in $Ik^{f/f}$ R26-$CreERT2^+$ (IKO) and $Ik^{f/f}$ R26-$CreERT2^-$ (WT) mice, injected with tamoxifen for 3 days, followed by 3 days of rest (**SI appendix, Fig. S3A**). This protocol did not alter the naive $CD4^+$ T cell compartment in numbers or phenotype (**SI appendix, Fig. S3B**). Naive $CD4^+$ T cells were stimulated with anti-CD3 and anti-CD28 Abs, in the absence or presence of IL-6 and increasing concentrations of TGFβ1, and IL-17 production was measured 3 days later (**Fig. 2A**). WT IL-17^+ cells were easily detected in wells with low concentrations of TGFβ1 (0.0017-0.03 ng/ml), and their numbers decreased as TGFβ1 concentrations went up, as expected *(35)*. In contrast, IKO IL-17^+ cells were barely detected in all conditions, similar to TKO cells. Thus, naive peripheral $CD4^+$ T cells need Ikaros to become Th17 cells.

High TGFβ1 concentrations induce the differentiation of $Foxp3^+$ regulatory T (Treg) cells *(36)*, and naive $CD4^+$ T cells may preferentially differentiate into Treg cells in the absence of Ikaros. We therefore measured the appearance of $Foxp3^+$ T cells in Th17 conditions, as described above. This showed that $Foxp3^+$ cells were produced in the WT samples at the higher TGFβ1 concentrations (0.5-8 ng/ml), but they were not observed in the IKO wells (**SI appendix, Fig. S3C**). Thus, Ikaros is required for the appearance of both Th17 and Treg cells following IL-6 and TGFβ1 stimulation.

As the mRNA of pro-inflammatory cytokines were upregulated in the Ikaros KO T cells, we assessed GM-CSF production in naive IKO CD4$^+$ T cells stimulated in Th0 or Th17 conditions. Strikingly, more IKO cells made GM-CSF, and more GM-CSF was made per cell, regardless of stimulation, and at all concentrations of TGFβ1 tested, compared with WT (**Fig. 2, B and C**). IKO CD4$^+$ T cells also produced more IFNγ (**SI appendix, Fig. S3D**), confirming a general deregulation of pro-inflammatory cytokine production in the absence of Ikaros. To determine if these results were due to Ikaros, or the indirect effects of IFNγ and IL-4 produced in these cultures *(37)*, we performed the experiments in the presence of neutralizing Abs against these cytokines. This treatment inhibited endogenous IFNγ production (**SI appendix, Fig. S3E**), but there was no detectable effect on the generation of IKO IL-17$^+$, Foxp3$^+$, or GM-CSF$^+$ cells (**SI appendix, Fig. S3, F-H**). Thus, Ikaros promotes IL-17 and inhibits pro-inflammatory cytokine production during Th17 polarization.

In the course of these experiments, we noticed more cell death in the Ikaros null cultures, a process that was reduced by the addition of the pan-caspase inhibitor QVD-OPh (**SI appendix, Fig. S4A**), suggesting death by apoptosis. Since *Fasl* mRNA was upregulated in stimulated TKO T cells (**Fig. 1C**), we asked if FasL signaling promoted Ikaros KO cell death, and perhaps the overproduction of GM-CSF$^+$ cells, since this pathway is associated with the production of pro-inflammatory cytokines *(38)*. To address these questions, we first measured *Fasl* mRNA in naive WT and IKO CD4$^+$ T cells after 0-2 days of culture in Th0 or Th17 conditions; *Fasl* mRNA was easily detected in the IKO cells within 1 day of stimulation in either condition compared with WT (**SI appendix, Fig. S4B**). Surface FasL was also increased on IKO cells (**SI appendix, Fig. S4C**). We then cultured naive WT and IKO CD4$^+$ T cells in Th0 conditions in the absence or presence of anti-FasL neutralizing Abs, and analyzed the cells for annexin V and propidium iodide positivity after 2 days. IKO cells had significantly less annexin V$^+$ cells when FasL signaling was blocked (**SI appendix, Fig. S4D**). To determine if FasL deregulation promotes GM-CSF expression in Ikaros null cells, we cultured naive WT and IKO T cells in Th0 conditions, in the presence of anti-FasL Abs, and measured GM-CSF expression. Interestingly, while the anti-FasL Ab blocked the appearance of WT GM-CSF$^+$ cells, as expected, it had little effect on IKO cells (**SI appendix, Fig. S4E**). Indeed, the number of IKO GM-CSF$^+$ cells seemed to increase when FasL signaling was blocked. Thus, Ikaros promotes cell survival by preventing *Fasl* upregulation, but blocks pro-inflammatory cytokine production via a different mechanism. In addition, QVD-OPh was included in the experiments below, unless specified, to maintain cell viability.

To determine if Ikaros is directly required during T cell polarization, we deleted *Ikzf1* in vitro, during the culture period, in CD4$^+$ T cells of untreated WT and IKO mice. Cells were

cultured in Th0 or Th17 conditions, and simultaneously treated with 4-hydroxytamoxifen (4-OHT) or ethanol (EtOH). Ikaros, GM-CSF and IL-17 expression were analyzed after 1-3 days of culture (**SI appendix, Fig. S5**). In these cultures, loss of Ikaros was observed in the large majority of cells after 2 days of 4-OHT treatment. GM-CSF was easily detected in the Ikaros$^{lo/-}$ IKO cells after 3 days of Th0 or Th17 stimulation compared with Ikaros sufficient cells (**SI appendix, Fig. S5A**), though it was less robust in the Th17 cultures, due probably to the inhibition of GM-CSF production by exogenous TGFβ1 *(8)*. In contrast, IL-17 production decreased with Ikaros loss in the IKO cells, starting at day 2 in Th17 conditions (**SI appendix, Fig. S5B**). These results indicated that Ikaros loss immediately results in the disappearance of cTh17 and the appearance of pTh17 cells. In a complementary experiment, we retrovirally expressed Ikaros (and GFP) or GFP only (pMIG) in naive WT and TKO CD4$^+$ T cells during Th0- or Th17-inducing conditions (**Fig. 2D**). In WT cells cultured in Th17 conditions, ectopic Ikaros slightly enhanced IL-17 production but had no effect on GM-CSF expression. In TKO cells, however, Ikaros re-expression rescued IL-17 production in Th17 conditions, and reduced GM-CSF in both Th0 and Th17 conditions. These results demonstrated that Ikaros promotes cTh17 polarization even in cells where Ikaros was deleted in the thymus.

To determine if T cell homeostasis in vivo is affected by Ikaros, we analyzed the T cell populations in TKO mice. Mutant mice showed decreases in total LN cellularity, and CD4$^+$ and CD8$^+$ T cell numbers, compared with WT (**SI appendix, Fig. S6, A and B**), though splenic T cells seemed unaffected. The frequencies of CD4$^+$ T cells were also lower. In contrast, B cell numbers were unchanged, but their frequencies were higher in the TKO LNs (**SI appendix, Fig. S6C**). In addition, naive TKO CD4$^+$ T cells were significantly decreased in numbers and frequencies compared with WT (**SI appendix, Fig. S6, D and E**), while TKO effector CD4$^+$ T cells were increased in frequencies (**SI appendix, Fig. S6F**). Interestingly, IL-7Rα levels were reduced on naive TKO CD4$^+$ T cells (**SI appendix, Fig. S4G**), suggesting a possible defect in cell survival. To determine if Ikaros null T cells produced more pro-inflammatory cytokines in vivo, we evaluated the production of IL-17 and GM-CSF in freshly isolated WT and TKO cells. These experiments indicated that more LN and splenic TKO CD4$^+$T cells, and not CD8$^+$, were consistently and selectively positive for GM-CSF (**Fig. 2E and SI appendix, Fig. S7A**). On the other hand, IL-17 production was increased only in frequency in TKO LN CD4$^+$ T cells (**SI appendix, Fig. S7B**). These results suggested that Ikaros deficiency is closely associated with an increase in GM-CSF production in vivo.

Altogether, our results showed that naive CD4$^+$ T cells can become IL-17- or GM-CSF-producing cells depending on the stimulation and their intrinsic levels of Ikaros — IL-

17 expression requires high Ikaros levels, while GM-CSF is induced in cells that have lost Ikaros.

Ikaros is essential to limit the pathogenic phenotype of CD4$^+$ T cells and promotes their proliferation upon activation

Because GM-CSF is induced in Ikaros null cells cultured in Th0 conditions, we explored its activation requirements. Naive WT and IKO CD4$^+$ T cells were isolated from tamoxifen-treated mice, and cultured in the absence of TCR stimulation (but maintained in IL-7 to help survival), with anti-CD3 Abs alone, or with anti-CD3 + anti-CD28 Abs. GM-CSF and IL-17 levels were measured over 3 days (**Figs. 3A and SI appendix Fig. S8A**). In the absence of TCR stimulation, WT and IKO cells did not make GM-CSF nor IL-17. Indeed, cells from either genotype did not make IL-17 in any of these conditions. However, some WT cells were GM-CSF$^+$ after 3 days of anti-CD3 + anti-CD28 stimulation. Strikingly, a large number of IKO cells made GM-CSF in response to either anti-CD3, or anti-CD3 + anti-CD28, at day 3. These results indicated that Ikaros null T cells needed only TCR stimulation to make GM-CSF, while WT cells required co-stimulatory CD28 signals, suggesting that Ikaros is required to set the activation threshold for pro-inflammatory cytokine production in CD4$^+$ T cells.

To determine why Ikaros null T cells respond so differently to TCR and CD28 stimulation, we analyzed the transcriptomes of naive WT and TKO CD4$^+$ T cells activated for 0-2 days in Th0 conditions, by RNA-sequencing. Three samples were analyzed per condition. Principal component analysis (PCA) of the expressed genes indicated that, globally, freshly isolated WT and TKO cells resembled each other, while activated cells of both genotypes clustered together (PC1; **Fig. 3B**), indicating that cell activation causes the biggest differences in gene expression. Among the upregulated genes upon T cell activation (**SI appendix, Fig. S8B**), some clusters (ie. 14, 18, 19) were less induced in the mutant cells. Similar results were observed among the downregulated genes (**SI appendix, Fig. S8C**), where genes from a few clusters were less downregulated (ie. 7, 9-11) in TKO cells. WT cells were also distinct from TKO cells (PC2; **Fig. 3B**). Differentially expressed genes that were upregulated only in the TKO cells included those that were also upregulated in Th17 conditions, such as genes encoding pro-inflammatory cytokines or their receptors (eg. *Csf2*, *Csf1*, *Ifng*, *Il23a*, *Il3*, *Il1a*, *Il15ra*, *Il2rb*), *Nlrp3*, associated with the inflammasome pathway, and *Foxo3* (**Fig. 3, C and D**). *Tbx21*, encoding Tbet, an activator of Th1 polarization, was also upregulated and Eomes, another member of the T-box superfamily, was less downregulated (Cluster 7, **SI appendix, Fig. S8C**), suggesting that transcriptomic signature of the mutant cells resemble the one of pTh1 cells. In direct correlation, metascape

analysis revealed the top pathways to be associated with cytokine signaling, actin cytoskeleton organization, and migration (**Fig. 3E and SI appendix Fig. S9**).

We also observed that cell cycle-related genes responded slower to activation, and were less upregulated, in Ikaros null cells compared with WT (cluster 18; **SI appendix, Fig. S8B**). This suggested that the proliferative response is impaired in the absence of Ikaros. To investigate this issue, we stimulated naive $CD4^+$ T cells from tamoxifen-treated WT and IKO mice in Th0 and Th17 conditions, and measured their division rates and kinetics of cytokine production. We found that IKO cells divided less than WT cells in both conditions, a phenotype that was most striking in Th0 conditions, where the majority of Ikaros null cells divided 2 cycles less than WT cells (**SI appendix, Fig. S10A**). To correlate cytokine production with cell cycle, we evaluated the percentage of GM-CSF^+ and IL-17^+ cells at every division after a 3 day culture. This showed that GM-CSF was detected in low-proliferating, while IL-17 was observed in high-proliferating, IKO cells (**SI appendix, Fig. S10, B and C**), revealing thus that IL-17 and GM-CSF are produced by different cell populations.

Together, these results indicate that Ikaros represses the appearance of a specific and distinct pro-inflammatory cytokine-producing $CD4^+$ T cell population in response to activation.

Loss of Ikaros alters the T cell epigenome

To determine how Ikaros influences chromatin accessibility, we studied the epigenome of WT and TKO $CD4^+$ T cells after Th0 activation over a 2-day period, by ATAC-sequencing. Three samples were analyzed for each condition. A total of 158,327 ATAC-seq peaks was identified for all conditions combined. The chromatin accessibility signatures of the different populations were analyzed by PCA (**Fig. 4A**), which separated the samples along lines similar to their RNA-seq profiles (**Fig. 3B**). Most of the ATAC-seq peaks were similar between WT and TKO chromatin (**Fig. 4B**), suggesting that they were Ikaros-independent. A small percentage showed increased or decreased accessibility in the TKO samples compared with WT, but the ratios of up vs. down were similar between different days of culture (**SI appendix Fig. S11A and Fig. 4C**). The genes with increased ATAC-seq peaks over time included many encoding pro-inflammatory cytokines, and *Fasl* (**SI appendix, Fig. S11B**). Most of the peaks were found in gene introns or intergenic regions and this was not changed with the loss of Ikaros (**SI appendix, Fig. S11C**). The majority of the regions with increased accessibility was correlated with genes whose expression levels were increased in the TKO cells (**SI appendix, Fig. S11D and Fig. 4D**), and included, among others, pro-inflammatory genes. Interestingly, the up and down changes in ATAC-seq peak signals were

frequently observed within the same locus, as was observed for the *Csf2*, *Fasl*, *Il3* and *Ifng* genes (**Fig. 4E and SI appendix Fig. S11E**), highlighting the complexity of gene regulation. Some of these changes were seen at day 0 in freshly isolated cells, while others were induced upon Th0 activation. These results indicated that increased chromatin accessibility correlates with increased gene expression in Ikaros null cells.

To determine if specific biological pathways are affected by Ikaros loss, we evaluated the ATAC-seq peaks that were greatly increased or decreased (Log_2FC TKO/WT >+2 or <-2; padj≤0.01) in these samples. Gene ontology analysis revealed that few pathways were significantly altered at d0 and after one day of activation (**SI appendix, Fig. S12A**). However, the genes associated with the STAT5 and NFκB pathways displayed some of the highest increases in ATAC-seq peak signals after 2 days of activation (**Fig. 4F**). We then searched for Ikaros, STAT5 and NFκB binding motifs under the peaks that were either increased (TKO), or decreased (WT), in TKO chromatin compared with WT. This showed that, under the peaks that were increased in TKO chromatin, the Ikaros and STAT5 motifs were selectively over-represented at all timepoints, while RelA (p65) motifs were over-represented only upon TCR + CD28 stimulation (**SI appendix Fig. S12B and Fig. 4G**). Together, these analyses suggest a molecular significance for Ikaros, STAT5 and RelA motifs in TKO cells.

Ikaros binding correlates with chromatin closing

To determine if the changes in chromatin accessibility were due to Ikaros, we analyzed Ikaros binding on the chromatin of naive WT cells, freshly isolated or activated in Th0 conditions for 1 day, by ChIP-sequencing. These analyses showed that the number and distribution of Ikaros peaks was similar in both conditions (**SI appendix, Fig. S13A**). Interestingly, the intensity of Ikaros binding was globally reduced upon activation (**Fig. 5A**). At regions where Ikaros bound to WT chromatin, we observed a significant increase in chromatin accessibility in TKO cells (**Fig. 5, A and B**), along with increases in gene expression (**Fig. 5C**). These results suggested that Ikaros binding correlates with chromatin compaction and gene repression. Nonetheless, our analysis of the Ikaros-bound regions at loci containing *Csf2*, *Ifng*, *Il7r, Fasl* and *Cish* (a positive control for Ikaros binding *(39)*) as well as those containing key regulatory proteins (ie. *Foxo3*, *Tbx21*, *Nfat5*, *Rorc*), did not reveal obvious differences in the levels of ATAC-seq peaks between WT and TKO chromatin (**Figs. 5D and SI appendix, Fig. S13B**). Thus, we concluded that Ikaros does not directly limit chromatin accessibility to repress a pro-inflammatory phenotype in activated T cells.

We found that Ikaros binds to the conserved non-coding sequence (CNSa), downstream of *Csf2*, which is an important enhancer for *Csf2* transcription *(20)* (**Fig. 5D**). To map the Ikaros binding site in this region, we performed an electrophoretic mobility shift assay (EMSA) with different probes containing the core Ikaros target motif GGAA. Of note, site 2 does not have an Ikaros core motif but corresponds to the summit of the Ikaros peak detected at d0. As positive controls, Ikaros strongly bound the synthetic BS4 and the *Cish* sequences. Interestingly, Ikaros bound efficiently to the probe containing a tandem of sites (sites 5 and 6) present in the CNSa **(Fig. 5E)**. Ikaros did not bind to site 4 alone. However, adding this sequence to the tandem sites promoted the appearance of a higher order complex, suggesting that additional proteins may be assembled with Ikaros. Mutagenesis analysis confirmed that sites 5 and 6 are crucial for Ikaros binding, while site 4 seems to be optional **(Fig. 5F)**. Thus, Ikaros binding to the CNSa occurs in a region containing a repetition of Ikaros core sequences.

Ikaros antagonizes STAT5- and NFκB-dependent GM-CSF production in activated T cells

Because Ikaros, STAT5 and RelA motifs were enriched at regions of increased accessibility in Ikaros KO chromatin, we investigated the relationship between Ikaros and these pathways in regulating pro-inflammatory cytokine production. To assess the importance of STAT5, we evaluated the levels of STAT5 and activated STAT5 (p-STAT5) in naive $CD4^+$ T cells from tamoxifen-treated WT and IKO mice, cultured for 2 days in Th0 conditions, by Western blot. Interestingly, p-STAT5 levels were increased approximately 3-fold in IKO cells (**Fig. 6A**). To determine if increased STAT5 activity influences GM-CSF expression, we cultured these cells in Th0 conditions, and a STAT5 inhibitor (STAT5i). Both *Csf2* mRNA and GM-CSF levels were reduced with increasing STAT5i concentrations (**Fig. 6, B and C**), suggesting that STAT5 activation plays a role in promoting GM-CSF production in Ikaros null cells.

To evaluate the importance of the NFκB pathway, we first treated WT and IKO cells with an inhibitor of IKK2 (IKK2i), a subunit of the IKK kinase that is required for the phosphorylation and degradation of the inhibitor of NFκB (IκBα) leading to NFκB activation. Strikingly, IKK2i treatment almost completely inhibited *Csf2* and GM-CSF expression in the activated IKO cells (**Fig. 6, D and E**). Similar results were obtained when we expressed a mutant IκBα protein that cannot be phosphorylated (IκBαSR), to block NFκB activation in WT and IKO cells (**Fig. 6F**). This showed that GM-CSF production was prevented >7-fold in activated IKO cells expressing IκBαSR (and GFP), suggesting a pivotal role for NFκB activation in boosting GM-CSF expression in the absence of Ikaros.

Together, these results indicated that Ikaros represses STAT5- and NFκB-dependent GM-CSF expression upon TCR and CD28 co-activation.

Reduced expression of Ikaros in human T cells leads to an increased GM-CSF production.

Finally, we asked if the function of Ikaros in inhibiting GM-CSF expression is conserved in human T cells. We activated peripheral blood lymphocytes (PBLs) from healthy donors with anti-CD3 ± anti-CD28 Abs, in the presence or absence of Lenalidomide, a drug causing Ikaros degradation *(40, 41)*. As expected, Ikaros expression was significantly decreased in Lenalidomide-treated cells (Fig. 7A). Strikingly, GM-CSF production and *CSF2* mRNA expression increased 2-3-fold in Lenalidomide-treated cells, respectively at d3 and d2 of the culture (**Figs. 7A and B**). These results therefore show that human T cells, like murine cells, require Ikaros to limit GM-CSF expression.

DISCUSSION

In this study, we reveal Ikaros as a central negative regulator of the production of pro-inflammatory cytokines, particularly GM-CSF, which is linked to T cell pathogenicity. Ikaros promotes cTh17 development from naive $CD4^+$ T cells, and is required during the polarization process. On the other hand, we find that Ikaros is required to suppress the development of pro-inflammatory T cells. In the absence of Ikaros, $CD4^+$ T cells polarized in Th17 cultures express pro-inflammatory cytokines resembling those expressed by pTh17, Th-GM and Th17 cells infiltrating the central nervous system during EAE. Further, Ikaros-mediated repression of the pathogenic phenotype is independent of the polarization towards the Th17 fate, as TCR and CD28 co-activation can also induce this phenotype. Indeed, upon T cell activation, Ikaros represses transcription via chromatin remodeling and target gene binding, including at the *Csf2* locus. Importantly, we show that Ikaros also represses GM-CSF expression in TCR/CD28-activated human T cells. Thus, Ikaros is intimately tied to the balance between the conventional versus pro-inflammatory/pathogenic T cell phenotype in response to antigen.

Upon TCR and CD28 activation, loss of Ikaros leads to high *Ifng*, *Foxo3, Tbx21* (encoding T-bet), and *Eomes* expression, in addition to that of *Csf2*. These genes have been described to drive Th1 pathogenicity in an EAE model *(9)*, suggesting that Ikaros may repress more than one type of pathogenic T cell. We found that Ikaros binds to the promoters or enhancers of all of these loci. Ikaros has been described as a repressor of *Tbx21* and *Ifng* expression during Th2 polarization *(42)*, but its potential role in limiting *Foxo3* and *Eomes* expression remains to be determined. We also observed that the activated Ikaros null T cells show an increased expression of *Maf* and *Prdm1,* which encode the Th2-associated factors Maf and Blimp-1, respectively. These transcriptional regulators have been shown to enhance *Csf2* expression *(43, 44)*. However, the expression of the genes encoding T-bet, Maf and Blimp-1 was unchanged between WT and KO cells in Th17 conditions, suggesting that these factors do not contribute to GM-CSF expression in this context. How cell fate cues and lineage specific transcriptional regulators interfere with Ikaros-dependent repression of the pro-inflammatory phenotype remains to be determined. Cell fate specific conditions may indeed modulate the expression of pathogenic cytokines, as GM-CSF expression was no longer induced when the cells were stimulated in the presence of high concentrations of TGFβ1.

Our results suggest that Ikaros might inhibit GM-CSF production at three junctures. First, Ikaros may cooperate with NFκB to regulate *Csf2* (and likely *Il3*) transcription. We show that Ikaros binds the CNSa sequence 34 kb downstream of the *Csf2* gene, a site that

was previously reported to be recognized by NFκB and Brg1 (a SWI/SNF remodeling ATPase) and important for *Il3* transcription *(20)*. Since Ikaros is already present at this site in naive $CD4^+$ T cells and remains there following TCR + CD28 activation, it might disturb the recruitment of NFκB and Brg1, which binds only after activation *(20)*. Second, Ikaros activity is negatively correlated with STAT5 phosphorylation, and active STAT5 is clearly required for strong GM-CSF expression in mutant cells, suggesting that Ikaros can affect the signaling cascades leading to STAT5 activation. As Ikaros binds close to the STAT5 *(45)* and NFκB *(20)* binding sites on the CNSa, it could potentially dislodge them from their target sites or inhibit their function upon binding on adjacent sites. Third, Ikaros expression is associated with reduced chromatin accessibility at the *Csf2* enhancer where NFAT and AP1 can bind *(19)*, even though Ikaros is not present at this region. However, by binding to distal regulatory regions, Ikaros could recruit the NuRD remodeling ATPase, Mi2β *(46)*, or Polycomb Repressive Complex 2 *(47)* to the enhancer to promote chromatin compaction. Thus, Ikaros could block the access of critical transcription factors to the enhancer of *Csf2* by multiple ways.

How do the GM-CSF-producing T cells observed here fit into the current paradigms of pathogenic T cells? Our results suggest that Ikaros negatively regulates the pathogenic gene expression programs of pTh17, Th-GM and pTh1 cells. In addition, under Th17 conditions, T cells lacking Ikaros, strongly resemble Th17 cells infiltrating the central nervous system of mice during EAE *(34)*. T cells expressing high levels of GM-CSF have been found in the cerebrospinal fluid of multiple sclerosis (MS) patients, and they have been shown to be pathogenic in murine EAE models *(10, 11, 29, 48)*. Moreover, recent studies have highlighted GM-CSF as an essential Th cytokine that contributes to neuroinflammation in MS patients *(12, 13)*. Importantly, we show that Ikaros also represses GM-CSF production in human T cells. It will thus be of major interest to evaluate the functional consequences of Ikaros deficiency in models of autoimmunity. Interestingly, single-nucleotide polymorphisms in the *IKZF1* gene have been associated with autoimmune diseases like systemic lupus erythematosus, inflammatory bowel disease and primary Sjögren's syndrome *(49-52)*, suggesting that genetic variations leading to changes in Ikaros levels may also contribute to the pathogenic programs in these patients. Lastly, pathogenic Th1 cells, expressing high levels of $GM\text{-}CSF^+$ and $IFN\gamma^+$ have been found in the blood of patients with severe forms of Covid-19, requiring intensive care *(14)*. These results could fit into our observation that Ikaros expression inversely correlates with the expression of a broad range of pro-inflammatory genes, including *Csf2* and *Ifng*. As such, Ikaros could be considered as an

early prognosis biomarker and screening T cells for its expression in from Covid-19 patients could help predict the severity of the immune response.

MATERIALS AND METHODS

Mice and ethics statement

Ikaros$^{f/f}$ Cre^{-}, Ikaros$^{f/f}$ CD4Cre^{+} mice and Ikaros$^{f/f}$ Rosa26-CreERT2^{+} mice were previously described and designated here as WT, TKO and IKO, respectively *(33)*. Although TKO mice die from T-cell acute lymphoblastic lymphomas/leukemias (T-ALL) at 4-6 months of age, the animals used here (5-8 weeks-old) showed no signs of transformation in the peripheral organs. Inducible deletion of the floxed alleles of *Ikzf1* was performed by injecting adult IKO mice intra-peritoneally with tamoxifen (75 mg/kg; T5648, Sigma-Aldrich) dissolved in sunflower oil every day for 3 days followed by 3 days of rest. TKO mice were 5-8 weeks old and IKO mice were 5-12 weeks old, backcrossed 5-12 generations on C57BL/6; all gave similar results. Mice were bred and maintained in SPF conditions until use. Animal procedures were approved by the IGBMC ethics committee and the Ministère de l'Enseignement Supérieur, de la Recherche et de l'Innovation (2012-096 and APAFIS#21777-2019082318358785v3). For the studies on human cells, buffy coats were obtained from the Etablissement Français du Sang Grand Est and an authorization for a scientific use was provided by the Bioethics Committee of the Ministère de l'Enseignement Supérieur, de la Recherche et de l'Innovation (#AC-2020-3991).

Antibodies, cytokines and reagents

Anti-CD4-AF700 (RM 4-5), anti-CD44-FITC (IM7), anti-CD62L-PECF594 (MEL-14), anti-GM-CSF-BV421 (MP1-22E9), anti-IFNγ-PECF594 (XMG 1.2), anti-NK1.1-PE (PK136), anti-TCR$\gamma\delta$-PE (GL3), anti-FasL (MFL3), anti-TCRβ-PerCPCy5.5 (H57-597), anti-CD16/CD32 (2.4G2), anti-human GM-CSF (BVD2-21C11), purified neutralizing anti-IL-4 (11B11) or anti-IFNγ (XMG1.2) Abs and GolgiPlug^{TM} were from BD Biosciences. Anti-CD8α-PerCPCy5.5 or APC-Fire 750 (53-6.7), anti-CD25-PE (PC61.5), anti-IL7Rα (A7-R34), purified anti-CD3 (2C11), anti-CD28 (37.51), anti-human CD3 (OKT3), anti-human CD28 (CD28.2), neutralizing anti-FasL (MFL4) Abs, the control isotype for anti-FasL Ab (clone HTK888), and Annexin V-FITC were from Biolegend. Anti-IL-17-eF660 (eBio17B7), anti-CD19-AF700 (1D3), and anti-Foxp3-FITC (FJK-16S) Abs were from eBiosciences. Anti-Ikaros (A3; rabbit polyclonal Ab against the Ikaros C-terminus) was produced in-house. Goat anti-Rabbit IgG (H+L) (F(ab')$_2$ fragment)-AF488 was from Jackson ImmunoResearch. Murine rIL-6 (IL-6) (216-16) and human rTGFβ1 (hTGFβ1) (100-21C) were from Peprotech. DAPI (D1306) was from Invitrogen. Phorbol 12-myristate 13-acetate (PMA; P8139), 4-hydroxytamoxifen (H-7904) and propidium iodide (81845) were from Sigma-Aldrich. Ionomycin was from Life

Technologies and QVD-OPh (A1901) was from ApexBio. IKK2 inhibitor (TPCA-1; T1452) and STAT5 inhibitor (573108) were from Sigma-Aldrich and Calbiochem, respectively.

Th0 and Th17 cultures

Cell suspensions were prepared from total (mesenteric and peripheral) lymph nodes and cells were stained with anti-CD16/CD32 blocking Abs, anti-CD4, anti-CD8, anti-CD44, anti-CD25, anti-NK1.1 and anti-TCR$\gamma\delta$ Abs in 1X PBS 10% FCS for 15 min on ice. Naive $CD4^+$ T cells ($CD4^+CD8^-CD44^{lo/-}CD25^-NK1.1^-TCR\gamma\delta^-$) were sorted on either a FACSAria™ II SORP or a FACS ARIA™ FUSION (BD Biosciences) cell sorter. Sort purity was >98%. Alternatively, $CD4^+$ T cells were enriched using the "Dynabeads untouched mouse CD4 cell" kit (Invitrogen), stained with anti-CD44, anti-CD25, anti-NK1.1 and anti-TCR$\gamma\delta$ Abs in 1X PBS 10% FCS for 15 min on ice and naive $CD4^+$ T cells were sorted as previously described *(35)*. Both protocols gave similar results for Th17 differentiation. For Th17 differentiation, naive $CD4^+$ T cells ($4x10^4$ cells/well) were activated with anti-CD3 and anti-CD28 (2 µg/ml each) Abs, both pre-coated overnight on a Nunc-immuno 96-well plate (Thermo Scientific), in the absence or presence of IL-6 (10 ng/ml) and various TGFβ1 concentrations (0.0017-8 ng/ml), in 200 µl of IMDM medium supplemented with 10% inactivated FCS, GlutaMAX™-I, 100 U/ml Penicillin, 100 µg/ml Streptomycin, non-essential amino acids, sodium pyruvate, 10 mM Hepes and β-mercaptoethanol (IMDM 10% FCS) as previously described *(35)*. Similar results were obtained between human and mouse TGFβ1. When mentioned, naive $CD4^+$ T cells were activated with plate-bound anti-CD3 and anti-CD28 (2 µg/ml each), with or without IL-6 (10 ng/ml) and TGFβ1 (0.03 ng/ml) corresponding to Th17 and Th0 culture conditions, respectively. Where indicated, neutralizing anti-FasL Ab (20 µg/ml), neutralizing anti-IL-4 and anti-IFNγ Abs (10 µg/ml each), the pan-caspase inhibitor (QVD-OPh, 20 µM) and IL-7 (20 ng/ml) were added on naive $CD4^+$ T cells at d0. At day 3, cells were stimulated with PMA plus ionomycin (0.5 µg/ml each) and GolgiPlug™ (1/1000) for 2h. When mentioned, cells were first stained with a Zombie Aqua™ fixable viability dye (Biolegend) according to the manufacturer's protocol and then stained with anti-CD4, anti-CD8 Abs, fixed and permeabilized using the Foxp3 Fixation/Permeabilization kit (eBiosciences), and stained with anti-IL-17, anti-GM-CSF, anti-IFNγ and anti-Foxp3 Abs (where indicated). Protein expression was analyzed on live cells using the cytometer LSRII (BD Biosciences).

Flow cytometry analyses of freshly-isolated cells

Cells were isolated from mesenteric and peripheral LN or spleen and were stimulated with PMA plus ionomycin (0.5 µg/ml each) and GolgiPlug™ (1/1000) for 2h at 37°C and stained

ACKNOWLEDGEMENTS

We thank the Chan-Kastner Lab for discussions; Claudine Ebel and Muriel Philipps for cell sorting help; Michael Gendron, Alexandre Vincent, William Magnant and Sylvie Falcone for mouse husbandry; the GenomEast platform, a member of the 'France Génomique' consortium (ANR-10-INSB-0009) for RNA-seq library preparation and sequencing; Doulaye Dembele for microarray data analysis and advice for statistical analyses; Christoph Borner for sharing plasmids and Anne Dejean for helpful comments and critical reading of the manuscript. **Funding:** This study was funded by a grant from Fondation ARC to CC, an Agence Nationale de la Recherche (ANR) grant ANR-17-CE15-0023-02 to SC, an Equipe Fondation pour la Recherche Médicale (FRM) grant EQU201903007812 to SC, the grant ANR-10-LABX-0030-INRT, a French State fund managed by the ANR under the program Investissements d'Avenir ANR-10-IDEX-0002-02, and an equipment grant from the Ligue Régionale contre le Cancer du Grand Est to SC. CB and GM were supported by pre-doctoral fellowships from the FRM (FDM20170637770) and the Ministère de l'Enseignement Supérieur, de la Recherche et de l'Innovation, respectively.

REFERENCES

1. I. Ivanov, B. Mckenzie, L. Zhou, C. Tadokoro, A. Lepelley, J. Lafaille, D. Cua, D. Littman, The Orphan Nuclear Receptor RORγt Directs the Differentiation Program of Proinflammatory IL-17+ T Helper Cells, *Cell* **126**, 1121–1133 (2006).

2. X. O. Yang, B. P. Pappu, R. Nurieva, A. Akimzhanov, H. S. Kang, Y. Chung, L. Ma, B. Shah, A. D. Panopoulos, K. S. Schluns, S. S. Watowich, Q. Tian, A. M. Jetten, C. Dong, T Helper 17 Lineage Differentiation Is Programmed by Orphan Nuclear Receptors RORα and RORγ, *Immunity* **28**, 29–39 (2008).

3. M. J. McGeachy, K. S. Bak-Jensen, Y. Chen, C. M. Tato, W. Blumenschein, T. McClanahan, D. J. Cua, TGF-β and IL-6 drive the production of IL-17 and IL-10 by T cells and restrain TH-17 cell–mediated pathology, *Nat Immunol* **8**, 1390–1397 (2007).

4. X. Wu, J. Tian, S. Wang, Insight Into Non-Pathogenic Th17 Cells in Autoimmune Diseases, *Front. Immun.* **9**, 5483–8 (2018).

5. K. Ghoreschi, A. Laurence, X.-P. Yang, C. M. Tato, M. J. McGeachy, J. E. Konkel, H. L. Ramos, L. Wei, T. S. Davidson, N. Bouladoux, J. R. Grainger, Q. Chen, Y. Kanno, W. T. Watford, H.-W. Sun, G. Eberl, E. M. Shevach, Y. Belkaid, D. J. Cua, W. Chen, J. J. O'shea, Generation of pathogenic TH17 cells in the absence of TGF-β signalling, *Nature* **467**, 967–971 (2010).

6. Y. Lee, A. Awasthi, N. Yosef, F. J. Quintana, S. Xiao, A. Peters, C. Wu, M. Kleinewietfeld, S. Kunder, D. A. Hafler, R. A. Sobel, A. Regev, V. K. Kuchroo, Induction and molecular signature of pathogenic TH17 cells, *Nat Immunol* **13**, 991–999 (2012).

7. L. Codarri, G. Gyülvészi, V. Tosevski, L. Hesske, A. Fontana, L. Magnenat, T. Suter, B. Becher, RORγt drives production of the cytokine GM-CSF in helper T cells, which is essential for the effector phase of autoimmune neuroinflammation, *Nat Immunol* **12**, 560–567 (2011).

8. M. El-Behi, B. Ciric, H. Dai, Y. Yan, M. Cullimore, F. Safavi, G.-X. Zhang, B. N. Dittel, A. Rostami, The encephalitogenicity of TH17 cells is dependent on IL-1- and IL-23-induced production of the cytokine GM-CSF, *Nat Immunol* **12**, 568–575 (2011).

9. C. Stienne, M. F. Michieletto, M. Benamar, N. Carrié, I. Bernard, X.-H. Nguyen, Y. Lippi, F. Duguet, R. S. Liblau, S. M. Hedrick, A. Saoudi, A. S. Dejean, Foxo3 Transcription Factor Drives Pathogenic T Helper 1 Differentiation by Inducing the Expression of Eomes, *Immunity* **45**, 774–787 (2016).

10. W. Sheng, F. Yang, Y. Zhou, H. Yang, P. Y. Low, D. M. Kemeny, P. Tan, A. Moh, M. H. Kaplan, Y. Zhang, X.-Y. Fu, STAT5 programs a distinct subset of GM-CSF-producing T helper cells that is essential for autoimmune neuroinflammation, *Cell Res* **24**, 1387–1402 (2014).

11. J. Rasouli, G. Casella, S. Yoshimura, W. Zhang, D. Xiao, J. Garifallou, M. V. Gonzalez, A. Wiedeman, A. Kus, E. R. Mari, P. Fortina, H. Hakonarson, S. A. Long, G.-X. Zhang, B. Ciric, A. Rostami, A distinct GM-CSF+ T helper cell subset requires T-bet to adopt a TH1 phenotype and promote neuroinflammation, *Sci Immunol* **5**, eaba9953 (2020).

12. J. Komuczki, S. Tuzlak, E. Friebel, T. Hartwig, S. Spath, P. Rosenstiel, A. Waisman, L. Opitz, M. Oukka, B. Schreiner, P. Pelczar, B. Becher, Fate-Mapping of GM-CSF

Expression Identifies a Discrete Subset of Inflammation-Driving T Helper Cells Regulated by Cytokines IL-23 and IL-1β, *Immunity* **50**, 1289–1304.e6 (2019).

13. E. Galli, F. J. Hartmann, B. Schreiner, F. Ingelfinger, E. Arvaniti, M. Diebold, D. Mrdjen, F. van der Meer, C. Krieg, F. A. Nimer, N. Sanderson, C. Stadelmann, M. Khademi, F. Piehl, M. Claassen, T. Derfuss, T. Olsson, B. Becher, GM-CSF and CXCR4 define a T helper cell signature in multiple sclerosis, *Nat Med* **25**, 1290–1300 (2019).

14. Y. Zhou, B. Fu, X. Zheng, D. Wang, C. Zhao, Y. Qi, R. Sun, Z. Tian, X. Xu, H. Wei, Pathogenic T-cells and inflammatory monocytes incite inflammatory storms in severe COVID-19 patients, *National Science Review* **7**, 998–1002 (2020).

15. A. Bonaventura, A. Vecchié, T. S. Wang, E. Lee, P. C. Cremer, B. Carey, P. Rajendram, K. M. Hudock, L. Korbee, B. W. Van Tassell, L. Dagna, A. Abbate, Targeting GM-CSF in COVID-19 Pneumonia: Rationale and Strategies, *Front. Immun.* **11**, 1625 (2020).

16. F. M. Lang, K. M. C. Lee, J. R. Teijaro, B. Becher, J. A. Hamilton, GM-CSF-based treatments in COVID-19: reconciling opposing therapeutic approaches, *Nat Rev Immunol* **20**, 507–514 (2020).

17. J. D. Fraser, A. Weiss, Regulation of T-cell lymphokine gene transcription by the accessory molecule CD28, *Mol Cell Biol* **12**, 4357–4363 (1992).

18. P. N. Cockerill, M. F. Shannon, A. G. Bert, G. R. Ryan, M. A. Vadas, The granulocyte-macrophage colony-stimulating factor/interleukin 3 locus is regulated by an inducible cyclosporin A-sensitive enhancer, *Proc Natl Acad Sci USA* **90**, 2466–2470 (1993).

19. C. S. Osborne, M. A. Vadas, P. N. Cockerill, Transcriptional regulation of mouse granulocyte-macrophage colony-stimulating factor/IL-3 locus, *J Immunol* **155**, 226–235 (1995).

20. A. L. Wurster, P. Precht, M. J. Pazin, NF-κB and BRG1 bind a distal regulatory element in the IL-3/GM-CSF locus, *Molecular Immunology* **48**, 2178–2188 (2011).

21. R. Schreck, P. A. Baeuerle, NF-kappa B as inducible transcriptional activator of the granulocyte-macrophage colony-stimulating factor gene, *Mol Cell Biol* **10**, 1281–1286 (1990).

22. F. Jenkins, P. N. Cockerill, D. Bohmann, M. F. Shannon, Multiple signals are required for function of the human granulocyte-macrophage colony-stimulating factor gene promoter in T cells, *J Immunol* **155**, 1240–1251 (1995).

23. S. R. Himes, L. S. Coles, R. Reeves, M. F. Shannon, High mobility group protein I(Y) is required for function and for c-Rel binding to CD28 response elements within the GM-CSF and IL-2 promoters, *Immunity* **5**, 479–489 (1996).

24. R. S. Thomas, M. J. Tymms, L. H. McKinlay, M. F. Shannon, A. Seth, I. Kola, ETS1, NFkappaB and AP1 synergistically transactivate the human GM-CSF promoter, *Oncogene* **14**, 2845–2855 (1997).

25. A. F. Holloway, S. Rao, X. Chen, M. F. Shannon, Changes in Chromatin Accessibility Across the GM-CSF Promoter upon T Cell Activation Are Dependent on Nuclear Factor κB Proteins, *J Exp Med* **197**, 413–423 (2003).

26. K. H. Brettingham-Moore, S. Rao, T. Juelich, M. F. Shannon, A. F. Holloway, GM-CSF promoter chromatin remodelling and gene transcription display distinct signal and transcription factor requirements, *Nucleic Acids Res* **33**, 225–234 (2005).

27. F. S. Poke, W. R. Upcher, O. R. Sprod, A. Young, K. H. Brettingham-Moore, A. F. Holloway, A. U. Khan, Ed. Depletion of c-Rel from Cytokine Gene Promoters Is Required for Chromatin Reassembly and Termination of Gene Responses to T Cell Activation, *PLOS one* **7**, e41734–13 (2012).

28. J. Yu, X. Zhou, M. Nakaya, W. Jin, X. Cheng, S.-C. Sun, T Cell–Intrinsic Function of the Noncanonical NF-κB Pathway in the Regulation of GM-CSF Expression and Experimental Autoimmune Encephalomyelitis Pathogenesis, *J Immunol* **193**, 422–430 (2014).

29. R. Noster, R. Riedel, M.-F. Mashreghi, H. Radbruch, L. Harms, C. Haftmann, H.-D. Chang, A. Radbruch, C. E. Zielinski, IL-17 and GM-CSF Expression Are Antagonistically Regulated by Human T Helper Cells, *Science Translational Medicine* **6**, 241ra80–241ra80 (2014).

30. L. Y. Wong, J. K. Hatfield, M. A. Brown, Ikaros Sets the Potential for Th17 Lineage Gene Expression through Effects on Chromatin State in Early T Cell Development, *Journal of Biological Chemistry* **288**, 35170–35179 (2013).

31. C. Lyon de Ana, K. Arakcheeva, P. Agnihotri, N. Derosia, S. Winandy, Lack of Ikaros Deregulates Inflammatory Gene Programs in T Cells, *The Journal of Immunology* **202**, 1112–1123 (2019).

32. J. J. Heller, H. Schjerven, S. Li, A. Lee, J. Qiu, Z. M. E. Chen, S. T. Smale, L. Zhou, Restriction of IL-22-Producing T Cell Responses and Differential Regulation of Regulatory T Cell Compartments by Zinc Finger Transcription Factor Ikaros, *The Journal of Immunology* **193**, 3934–3946 (2014).

33. A.-S. Geimer Le Lay, A. Oravecz, J. Mastio, C. Jung, P. Marchal, C. Ebel, D. Dembele, B. Jost, S. Le Gras, C. Thibault, T. Borggrefe, P. Kastner, S. Chan, The Tumor Suppressor Ikaros Shapes the Repertoire of Notch Target Genes in T Cells, *Science Signaling* **7**, ra28 (2014).

34. R. Qiu, X. Yu, L. Wang, Z. Han, C. Yao, Y. Cui, G. Hou, D. Dai, W. Jin, N. Shen, Inhibition of Glycolysis in Pathogenic TH17 Cells through Targeting a miR-21-Peli1-c-Rel Pathway Prevents Autoimmunity, *The Journal of Immunology* **204**, 3160–3170 (2020).

35. A. Lainé, B. Martin, M. Luka, L. Mir, C. Auffray, B. Lucas, G. Bismuth, C. Charvet, Foxo1 Is a T Cell-Intrinsic Inhibitor of the RORγt-Th17 Program, *The Journal of Immunology* **195**, 1791–1803 (2015).

36. L. Zhou, J. E. Lopes, M. M. W. Chong, I. I. Ivanov, R. Min, G. D. Victora, Y. Shen, J. Du, Y. P. Rubtsov, A. Y. Rudensky, S. F. Ziegler, D. R. Littman, TGF-β-induced Foxp3 inhibits TH17 cell differentiation by antagonizing RORγt function, *Nature* **453**, 236–240 (2008).

37. L. E. Harrington, R. D. Hatton, P. R. Mangan, H. Turner, T. L. Murphy, K. M. Murphy, C. T. Weaver, Interleukin 17-producing CD4+ effector T cells develop via a lineage distinct from the T helper type 1 and 2 lineages, *Nat Immunol* **6**, 1123–1132 (2005).

38. S. P. Cullen, C. M. Henry, C. J. Kearney, S. E. Logue, M. Feoktistova, G. A. Tynan, E. C. Lavelle, M. Leverkus, S. J. Martin, Fas/CD95-Induced Chemokines Can Serve as ``Find-Me“” Signals for Apoptotic Cells, *Mol Cell* **49**, 1034–1048 (2013).

39. C. D. S. Katerndahl, L. M. Heltemes-Harris, M. J. L. Willette, C. M. Henzler, S. Frietze, R. Yang, H. Schjerven, K. A. T. Silverstein, L. B. Ramsey, G. Hubbard, A. D. Wells, R. P. Kuiper, B. Scheijen, F. N. van Leeuwen, M. Müschen, S. M. Kornblau, M. A. Farrar, Antagonism of B cell enhancer networks by STAT5 drives leukemia and poor patient survival, *Nat Immunol* **18**, 694–704 (2017).

40. J. Krönke, N. D. Udeshi, A. Narla, P. Grauman, S. N. Hurst, M. McConkey, T. Svinkina, D. Heckl, E. Comer, X. Li, C. Ciarlo, E. Hartman, N. Munshi, M. Schenone, S. L. Schreiber, S. A. Carr, B. L. Ebert, Lenalidomide Causes Selective Degradation of IKZF1 and IKZF3 in Multiple Myeloma Cells, *Science* **343**, 301–305 (2014).

41. G. Lu, R. E. Middleton, H. Sun, M. V. Naniong, C. J. Ott, C. S. Mitsiades, K.-K. Wong, J. E. Bradner, W. G. Kaelin Jr, The myeloma drug lenalidomide promotes the cereblon-dependent destruction of Ikaros proteins, *Science* **343**, 305–309 (2014).

42. R. M. Thomas, C. Chen, N. Chunder, L. Ma, J. Taylor, E. J. Pearce, A. D. Wells, Ikaros Silences T-bet Expression and Interferon-gamma Production during T Helper 2 Differentiation, *Journal of Biological Chemistry* **285**, 2545–2553 (2010).

43. J. Gilmour, D. J. Cousins, D. F. Richards, Z. Sattar, T. H. Lee, P. Lavender, Regulation of GM-CSF expression by the transcription factor c-Maf, *Journal of Allergy and Clinical Immunology* **120**, 56–63 (2007).

44. R. Jain, Y. Chen, Y. Kanno, B. Joyce-Shaikh, G. Vahedi, K. Hirahara, W. M. Blumenschein, S. Sukumar, C. J. Haines, S. Sadekova, T. K. McClanahan, M. J. McGeachy, J. J. O'shea, D. J. Cua, Interleukin-23-Induced Transcription Factor Blimp-1 Promotes Pathogenicity of T Helper 17 Cells, *Immunity* **44**, 131–142 (2016).

45. P. Li, S. Mitra, R. Spolski, J. Oh, W. Liao, Z. Tang, F. Mo, X. Li, E. E. West, D. Gromer, J.-X. Lin, C. Liu, Y. Ruan, W. J. Leonard, STAT5-mediated chromatin interactions in superenhancers activate IL-2 highly inducible genes: Functional dissection of the Il2ra gene locus, *Proceedings of the National Academy of Sciences* **114**, 12111–12119 (2017).

46. J. Kim, S. Sif, B. Jones, A. Jackson, J. Koipally, E. Heller, S. Winandy, A. Viel, A. Sawyer, T. Ikeda, R. Kingston, K. Georgopoulos, Ikaros DNA-binding proteins direct formation of chromatin remodeling complexes in lymphocytes, *Immunity* **10**, 345–355 (1999).

47. A. Oravecz, A. Apostolov, K. Polak, B. Jost, S. Le Gras, S. Chan, P. Kastner, Ikaros mediates gene silencing in T cells through Polycomb repressive complex 2, *Nature Communications* **6**, 1–15 (2015).

48. J. Zhang, A. I. Roberts, C. Liu, G. Ren, G. Xu, L. Zhang, S. Devadas, Y. Shi, A novel subset of helper T cells promotes immune responses by secreting GM-CSF, *Cell Death Differ* **20**, 1731–1741 (2013).

49. D. S. Cunninghame Graham, D. L. Morris, T. R. Bhangale, L. A. Criswell, A.-C. Syvänen, L. Rönnblom, T. W. Behrens, R. R. Graham, T. J. Vyse, M. I. McCarthy, Ed. Association of NCF2, IKZF1, IRF8, IFIH1, and TYK2 with Systemic Lupus Erythematosus, *PLoS Genet* **7**, e1002341 (2011).

50. J.-W. Han, H.-F. Zheng, Y. Cui, L.-D. Sun, D.-Q. Ye, Z. Hu, J.-H. Xu, Z.-M. Cai, W. Huang, G.-P. Zhao, H.-F. Xie, H. Fang, Q.-J. Lu, J.-H. Xu, X.-P. Li, Y.-F. Pan, D.-Q. Deng, F.-Q. Zeng, Z.-Z. Ye, X.-Y. Zhang, Q.-W. Wang, F. Hao, L. Ma, X.-B. Zuo, F.-S. Zhou, W.-H. Du, Y.-L. Cheng, J.-Q. Yang, S.-K. Shen, J. Li, Y.-J. Sheng, X.-X. Zuo, W.-F. Zhu, F. Gao, P.-L. Zhang, Q. Guo, B. Li, M. Gao, F.-L. Xiao, C. Quan, C. Zhang, Z. Zhang, K.-J. Zhu, Y. Li, D.-Y. Hu, W.-S. Lu, J.-L. Huang, S.-X. Liu, H. Li, Y.-Q. Ren, Z.-X. Wang, C.-J. Yang, P.-G. Wang, W.-M. Zhou, Y.-M. Lv, A.-P. Zhang, S.-Q. Zhang, D. Lin, Y. Li, H. Q. Low, M. Shen, Z.-F. Zhai, Y. Wang, F.-Y. Zhang, S. Yang, J.-J. Liu, X.-J. Zhang, Genome-wide association study in a Chinese Han population identifies nine new susceptibility loci for systemic lupus erythematosus, *Nat. Genet.* **41**, 1234–1237 (2009).

51. V. Gateva, J. K. Sandling, G. Hom, K. E. Taylor, S. A. Chung, X. Sun, W. Ortmann, R. Kosoy, R. C. Ferreira, G. Nordmark, I. Gunnarsson, E. Svenungsson, L. Padyukov, G. Sturfelt, A. Jönsen, A. A. Bengtsson, S. Rantapää-Dahlqvist, E. C. Baechler, E. E. Brown, G. S. Alarcón, J. C. Edberg, R. Ramsey-Goldman, G. McGwin, J. D. Reveille, L. M. Vilá, R. P. Kimberly, S. Manzi, M. A. Petri, A. Lee, P. K. Gregersen, M. F. Seldin, L. Rönnblom, L. A. Criswell, A.-C. Syvänen, T. W. Behrens, R. R. Graham, A large-scale replication study identifies TNIP1, PRDM1, JAZF1, UHRF1BP1 and IL10 as risk loci for systemic lupus erythematosus, *Nat. Genet.* **41**, 1228–1233 (2009).

52. S. Qu, Y. Du, S. Chang, L. Guo, K. Fang, Y. Li, F. Zhang, K. Zhang, J. Wang, L. Prokunina-Olsson, Ed. Common variants near IKZF1 are associated with primary Sjögren's syndrome in Han Chinese, *PLOS one* **12**, e0177320 (2017).

FIGURE LEGENDS

Figure 1. Loss of Ikaros induces a pathogenic gene expression program.

(A) Left: representative contour plots of IL-17 and CD4 expression in WT and TKO $CD4^+$ cells stimulated for 3d in Th17 or Th0 conditions. Right: proportion of WT or TKO $IL\text{-}17^+$ cells among $CD4^+$ cells from 3d in Th17 cultures (n=5; mean ± SEM). **(B)** Principal component analysis using expression data (microarray) from WT and TKO $CD4^+$ cells at d0 and d1-2 in Th17 cultures. The graph shows the first two principal components. **(C)** Heat maps of 3 clusters of genes that were specifically increased in TKO cells compared to WT (K-means clustering). **(D)** RT-qPCR analysis of *Csf2*, *Ifng*, *Il3* and *Il10* mRNA expression in either naive $CD4^+$ T cells (d0) or naive $CD4^+$ T cells cultured in Th17 polarizing condition with QVD-OPh for 1 or 2 days (n=5; mean ± SEM). **(E)** Metascape analysis of GO term enrichment of genes in cluster 1-3 described in C. **(F)** GSEA enrichment plots of genes enriched in pathogenic Th17 cells (pTh17; top) or conventional Th17 cells (cTh17; bottom) among genes up- or down-regulated by Ikaros at d1. Gene sets correspond to 106 genes enriched in pTh17 cells and 143 genes enriched in cTh17 cells *(6)*. NES, normalized enrichment score; FDR, false discovery rate. Statistical significance was analyzed by a Mann-Whitney test (*p ≤0.05 and **p ≤0.01).

Figure 2. Ikaros limits the expression of GM-CSF in Th17 polarizing conditions.

(A) Left: representative graph of the proportions of $IL\text{-}17^+$ cells in activated WT and IKO naive LN $CD4^+$ T cells cultured with anti-CD3 and anti-CD28 Abs and different amounts of TGFβ1 and constant IL-6 for 3 days, as indicated. Right: graph showing the proportions of WT and IKO $IL\text{-}17^+$ cells among $CD4^+$ T cells in 3d cultures, as indicated (n=5; mean ± SEM). **(B)** Representative contour plot showing IL-17 and GM-CSF expression in WT and IKO $CD4^+$ cells after 3 days of culture in Th0 or Th17 conditions. **(C)** Left: representative graph showing the percentage of $GM\text{-}CSF^+$ cells in WT and IKO LN $CD4^+$ cells cultured as in A. Right: graph showing the proportions of $GM\text{-}CSF^+$ $CD4^+$ T cells (n=5; mean ± SEM). **(D)** Naive LN $CD4^+$ T cells from WT and TKO mice, cultured in Th0 or Th17 conditions for 24h and subjected to 2 rounds of infection with pMIG or Ikaros/pMIG in the presence of QVD-OPh. Representative panel of GFP expression at d3, and expression of IL-17 and GM-CSF in live GFP^+ cells in Th0 (left) or Th17 (right) condition (n=2). **(E)** Left panels: Representative contour plot of ex vivo GM-CSF-expressing cells in WT and TKO $CD4^+$ T cells in LN and spleen. Middle panel: percentage of $GM\text{-}CSF^+$ cells among $CD4^+$ T cells from LN (n=10) or spleen (n=9) from WT and TKO mice. Right panel: cell counts of $GM\text{-}CSF^+$ cells among WT and TKO $CD4^+$ T cells from LN (n=10) or spleen (n=9) of WT and

TKO mice (mean ± SEM). Statistical significance was analyzed by a Mann-Whitney test (*p ≤ 0.05, **p ≤ 0.01, ***p≤ 0.001).

Figure 3. Ikaros is required to limit GM-CSF expression upon T cell activation by TCR and CD28 signals.

(A) Naive WT and IKO LN $CD4^+$ cells from tamoxifen-induced mice were cultured with IL-7, or activated with anti-CD3 ± anti-CD28 Abs for 1-3 days in the presence of QVD-OPh. Representative contour plot showing GM-CSF and IL-17 expression in live $CD4^+$ cells (n=4). **(B)** Principal component analysis using expression data (RNA-seq) from WT and TKO T $CD4^+$ cells at d0 and d1-2 in Th0 cultures. The graph shows the first two principal components. **(C)** Heat maps of 3 clusters of genes that were specifically increased in TKO cells compared to WT in Th0 cultures (K-means clustering). **(D)** Heat map of a cluster of genes more increased in TKO cells compared to WT in Th0 cultures at d1 and 2 (K-means clustering). **(E)** Metascape analysis of GO term enrichment of genes from cluster 4 in panel D.

Figure 4. Ikaros loss changes the landscape of chromatin accessibility in $CD4^+$ T cells.

(A) Principal component analysis using ATAC-seq data from WT and TKO $CD4^+$ cells at d0 and d1-2 in Th0 cultures. The graph shows the first two principal components. Samples were obtained from three independent experiments. **(B)** Pie chart showing the distribution of ATAC-seq peaks in TKO cells compared to WT cells at d0 and d1-2 in Th0 cultures. Peaks increased in TKO cells (black; Log_2FC TKO/WT>1 and padj≤0.01) or decreased in TKO cells (white; Log_2FC TKO/WT<-1 and padj≤0.01). The peaks that are not significantly changed between WT and TKO samples are shown in grey. **(C)** SeqMINER heat map of all the 87221 ATAC-seq peaks in WT and TKO cells at d2 of Th0 cultures. **(D)** Integration of RNA-seq data with ATAC-seq data from TKO cells compared to WT cells at d2 of Th0 cultures. Only the 8572 peaks with a padj ≤ 0.05 from the ATAC-seq and RNA-seq analysis are shown. Among them, 3576 peaks have a Log_2FC (TKO/WT) ≥ 1 or ≤ -1 and a Pearson correlation coefficient of 0.58 with a p value< 2.2^{-16}. Genes with a positive (purple) or a negative (black) correlation between ATAC-seq and RNA-seq data are highlighted. **(E)** Genome track view of ATAC-seq profiles of *Csf2* and *Fasl*. The University of California Santa Cruz Genome browser (UCSC) depicts the pooled profile of the three independent experiments in WT and TKO $CD4^+$ T cells at d0 and d1-2 in Th0 cultures. **(F)** Heat map showing GO terms enriched within genes associated with 4486 ATAC-seq peaks significantly increased and 2774 peaks significantly decreased in TKO $CD4^+$ T cells in comparison to WT $CD4^+$ T cells at d2 in Th0 cultures. Peaks significantly increased or decreased in the TKO were defined respectively

with the following criteria: (Log_2FC(TKO/WT) > 2 with a padj ≤ 0.01), and (Log_2FC(TKO/WT) < -2 with a padj ≤ 0.01). **(G)** Bar graph showing the significantly enriched transcription factor motifs identified from AME-MEME motif search in ATAC-seq peaks found in WT and TKO $CD4^+$ T cells at d2 in Th0 cultures. Significant peaks were selected as in F. Only some of the significantly enriched motifs are depicted.

Figure 5. Genome-wide ChIP-seq analysis of Ikaros binding in $CD4^+$ T cells.

(A) SeqMINER heat map showing the Ikaros peaks and the ATAC-seq peaks at d0 and d1 of Th0 cultures. **(B)** Boxplot showing the Log_2FC (TKO/WT) of all ATAC-seq peaks (78378) in TKO versus WT cells that were bound (26054) or not (52324) by Ikaros in the Th0 d1 condition (Mann-Whitney test, $p<2.2^{-16}$). **(C)** Integration of ATAC-seq data (Log_2FC TKO/WT) and RNA-seq data (Log_2FC TKO/WT) among the regions directly bound by Ikaros (26054 peaks) at d1 of Th0 culture. Gray dots: ATAC-seq regions with a more significant difference in accessibility between TKO and WT (padj ≤ 0.05) associated with a difference in the RNA-seq expression (padj ≤ 0.05). Red dots: ATAC-seq Log_2FC (TKO/WT) ≥ 1 and RNA-seq Log_2FC (TKO/WT) ≥1. Blue dots: ATAC-seq Log_2FC (TKO/WT) ≥ 1 and RNA-seq Log_2FC (TKO/WT) ≤ -1. Black dots: ATAC-seq Log_2FC (TKO/WT) ≤ -1 and RNA-seq Log_2FC (TKO/WT) ≤ -1 or ≥ 1. **(D)** UCSC Genome track view of Ikaros ChIP-seq profiles, showing the *Csf2* promoter and regulatory sequences in WT $CD4^+$ T cells at d0 and d1 of Th0 cultures and ATAC-seq of WT and TKO $CD4^+$ T cells at d0 and d1-2 in Th0 cultures. CNSa is shown on the left and a focus on the *Csf2* promoter and enhancer is shown on the right. **(E)** Binding of Ikaros to sites identified in the CNSa of the *Csf2* gene. Sites 2 and 3 correspond respectively to the summits of the Ikaros peak at d0 and Th0 d1. BS4 and Cish probes are used as positive controls. Nuclear extracts from Cos cells transfected with the empty vector were used as a negative control (Mock). **(F)** Analysis of Ikaros binding on CNSa probes with mutations on sites 4-6.

Figure 6. GM-CSF production in Ikaros-deficient $CD4^+$ T cells depends on STAT5 and NFκB.

(A) Left: Western blot of Ikaros and the phosphorylation of STAT5-Y694 in WT and IKO $CD4^+$ cells cultured 2 days in Th0 conditions with QVD-OPh. Tubulin and STAT5 are shown as loading controls. Right: Ratio of STAT5-pY694/STAT5 in WT and IKO $CD4^+$ T cells at d2 of Th0 cultures with QVD-Oph (n=4; mean ± SEM). **(B)** Naive LN WT and IKO $CD4^+$ cells from tamoxifen-induced mice were cultured in Th0 conditions for 3 days with QVD-OPh in the presence of the STAT5 inhibitor (STAT5i) at indicated concentrations or DMSO as a

control. Left: Representative contour plot showing GM-CSF and IL-17 expression in WT and IKO $CD4^+$ cells. Right: Proportion of WT and IKO GM-CSF^+ $CD4^+$ T cells after 3 days of Th0 culture (n=4-5; mean ± SEM). **(C)** RT-qPCR analysis of *Csf2* mRNA expression in WT and IKO LN naive $CD4^+$ cells cultured in Th0 conditions with QVD-OPh (d2) in the presence of DMSO or STAT5i at indicated concentrations. *Csf2* mRNA expression is represented as -fold induction with respect to the DMSO WT sample. Statistical significance for WT and IKO DMSO condition was analyzed by a Wilcoxon test. **(D)** Naive LN $CD4^+$ cells from tamoxifen-induced WT and IKO mice were cultured in Th0 conditions for 3 days with QVD-OPh in the presence of the IKK2 inhibitor (IKK2i; 2.5 µM) or DMSO as a control. Left: Representative contour plot showing GM-CSF and IL-17 expression in WT and IKO $CD4^+$ cells. Right: Proportion of WT and IKO GM-CSF^+ $CD4^+$ T cells after 3 days of Th0 culture with DMSO or IKK2i (n=6; mean ± SEM)**. (E)** RT-qPCR analysis of *Csf2* mRNA expression in naive LN WT and IKO $CD4^+$ cells harvested at d0 or cultured in Th0 conditions with QVD-OPh (d2) in the presence of DMSO or IKK2i (2.5 µM) and neutralizing anti-IFNγ and anti-IL-4 Abs (10 µg/ml). *Csf2* mRNA expression is represented as -fold induction with respect to the DMSO WT sample (n=4; mean ± SEM)**. (F)** Naive LN $CD4^+$ T cells from tamoxifen-induced WT and IKO mice were activated with anti-CD3 + anti-CD28 Abs for 24h and subjected to 2 rounds of infection with pMIG or IκBα super repressor (SR)/pMIG in the presence of QVD-OPh. At d3, cells were stimulated with PMA, ionomycin and Golgiplug for 2h, and IL-17 and GM-CSF expression was analyzed. Top: Representative panels of GFP expression and of IL-17 and GM-CSF expression in GFP^- and GFP^+ cells are shown. Bottom: Proportion of WT and IKO GM-CSF^+ $CD4^+$ T cells infected with pMIG or IκBα super repressor after 3 days of Th0 culture (n=3; mean ± SEM). Statistical significance was analyzed by parametric unpaired t-test. Unless otherwise specified, statistical significance was analyzed by a Mann-Whitney test (*$p \leq 0.05$, **$p \leq 0.01$, ***$p \leq 0.001$).

Figure 7. Human cells require Ikaros to limit GM-CSF expression.

PBMCs were isolated from buffy coats of healthy donors and activated on not with anti-CD3 ± anti-CD28 Abs (10 µg/ml each) in the presence of Lenalidomide (10 µM) or DMSO as a control. **(A)** Left: Representative dot plot showing Ikaros and GM-CSF expression in DMSO and Lenalidomide-treated cells after 3 days of culture, upon T cell activation or not. Middle: Mean Fluorescence Intensity (MFI) of Ikaros (n=4; mean ± SEM). Right: Proportion of GM-CSF^+ cells (n=4; mean ± SEM). Statistical significance was analyzed by a paired student t-test (*$p \leq 0.05$). (B) RT-qPCR analysis of *CSF2* mRNA expression at d2 of culture in DMSO and Lenalidomide-treated cells upon T cell activation or not (n=2; mean ± SEM).

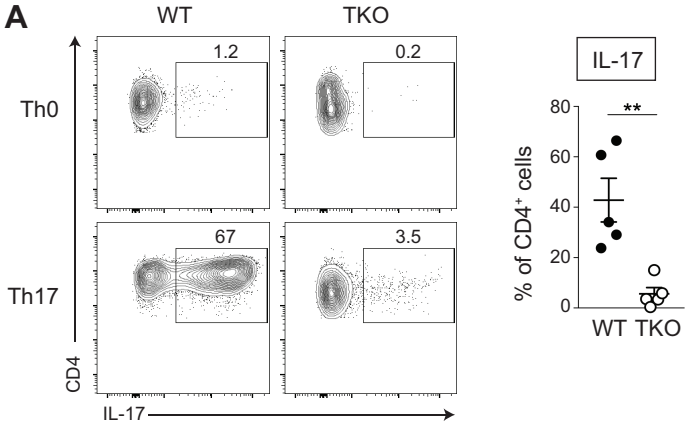
A
WT
TKO
Th0
Th17
1.2
0.2
67
3.5
CD4
IL-17
IL-17
% of CD4+ cells
**
WT TKO

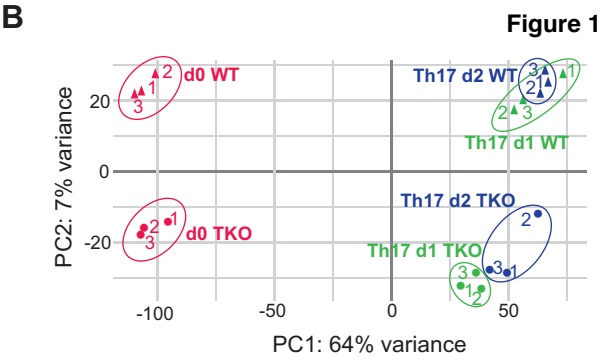
B
d0 WT
Th17 d2 WT
Th17 d1 WT
d0 TKO
Th17 d2 TKO
Th17 d1 TKO
PC2: 7% variance
PC1: 64% variance

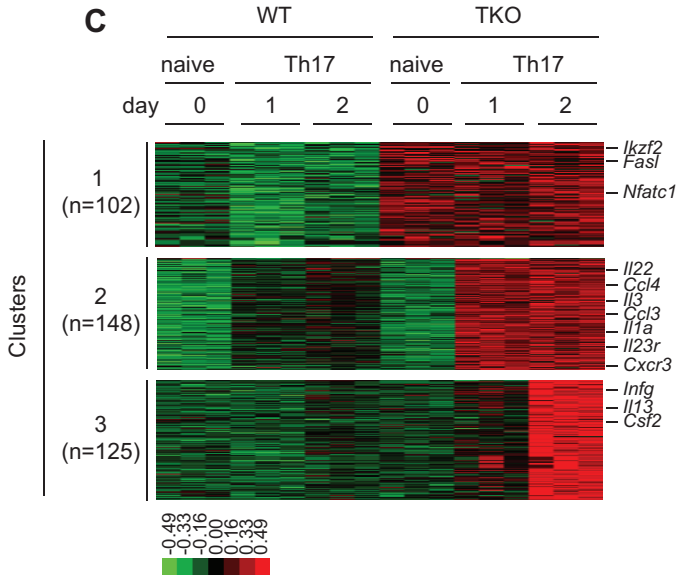
C
WT
TKO
naive
Th17
day
Clusters
1 (n=102)
2 (n=148)
3 (n=125)
Ikzf2
Fasl
Nfatc1
Il22
Ccl4
Il3
Ccl3
Il1a
Il23r
Cxcr3
Ifng
Il13
Csf2
-0.49 -0.33 -0.16 0.00 0.16 0.33 0.49

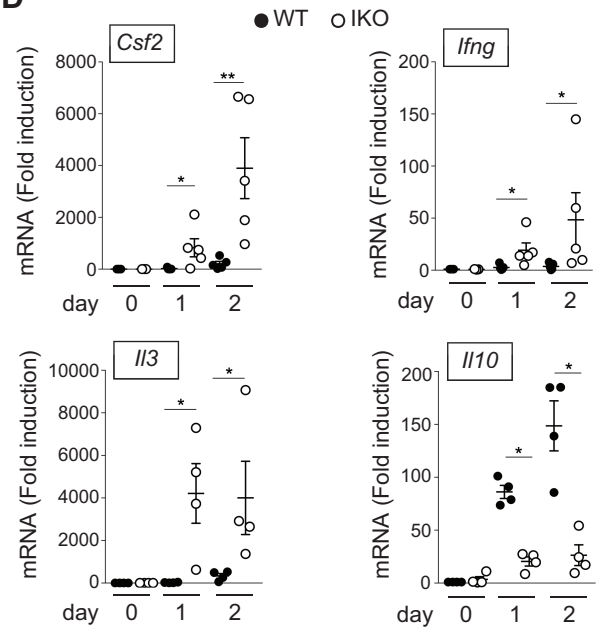
D
WT
IKO
Csf2
Ifng
Il3
Il10
mRNA (Fold induction)
day

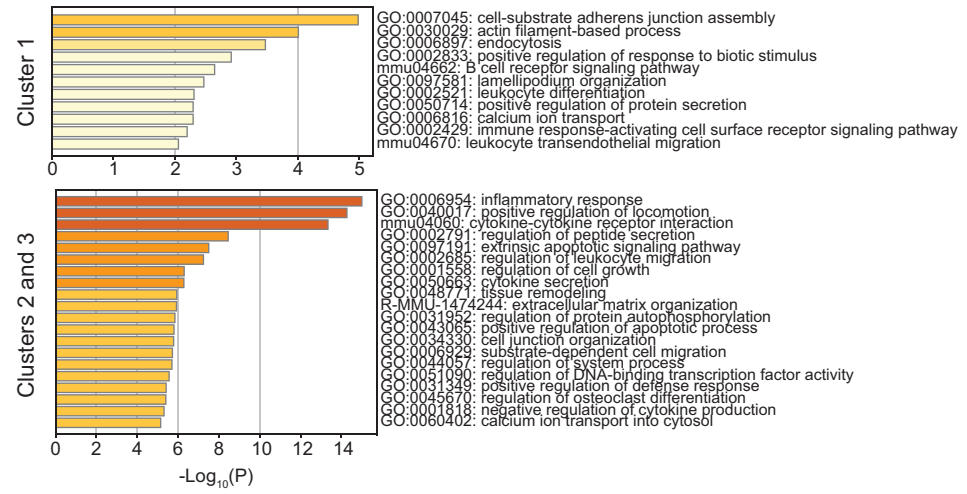
E
Cluster 1
GO:0007045: cell-substrate adherens junction assembly
GO:0030029: actin filament-based process
GO:0006897: endocytosis
GO:0002833: positive regulation of response to biotic stimulus
mmu04662: B cell receptor signaling pathway
GO:0097581: lamellipodium organization
GO:0002521: leukocyte differentiation
GO:0050714: positive regulation of protein secretion
GO:0006816: calcium ion transport
GO:0002429: immune response-activating cell surface receptor signaling pathway
mmu04670: leukocyte transendothelial migration
Clusters 2 and 3
GO:0006954: inflammatory response
GO:0040017: positive regulation of locomotion
mmu04060: cytokine-cytokine receptor interaction
GO:0002791: regulation of peptide secretion
GO:0097191: extrinsic apoptotic signaling pathway
GO:0002685: regulation of leukocyte migration
GO:0001558: regulation of cell growth
GO:0050663: cytokine secretion
GO:0048771: tissue remodeling
R-MMU-1474244: extracellular matrix organization
GO:0031952: regulation of protein autophosphorylation
GO:0043065: positive regulation of apoptotic process
GO:0034330: cell junction organization
GO:0006929: substrate-dependent cell migration
GO:0044057: regulation of system process
GO:0051090: regulation of DNA-binding transcription factor activity
GO:0031349: positive regulation of defense response
GO:0045670: regulation of osteoclast differentiation
GO:0001818: negative regulation of cytokine production
GO:0060402: calcium ion transport into cytosol
-Log10(P)

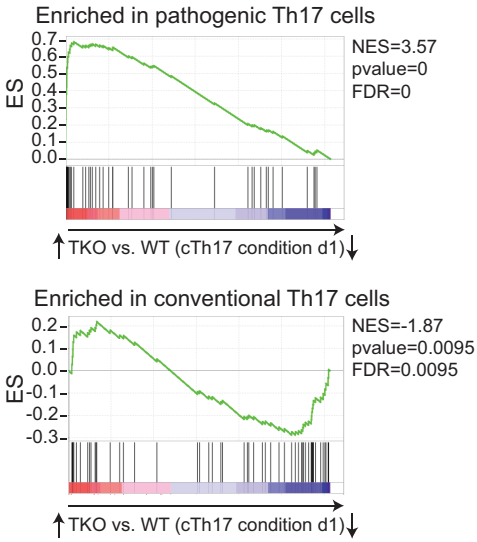
F
Enriched in pathogenic Th17 cells
NES=3.57
pvalue=0
FDR=0
ES
TKO vs. WT (cTh17 condition d1)
Enriched in conventional Th17 cells
NES=-1.87
pvalue=0.0095
FDR=0.0095
ES
TKO vs. WT (cTh17 condition d1)

Figure 2

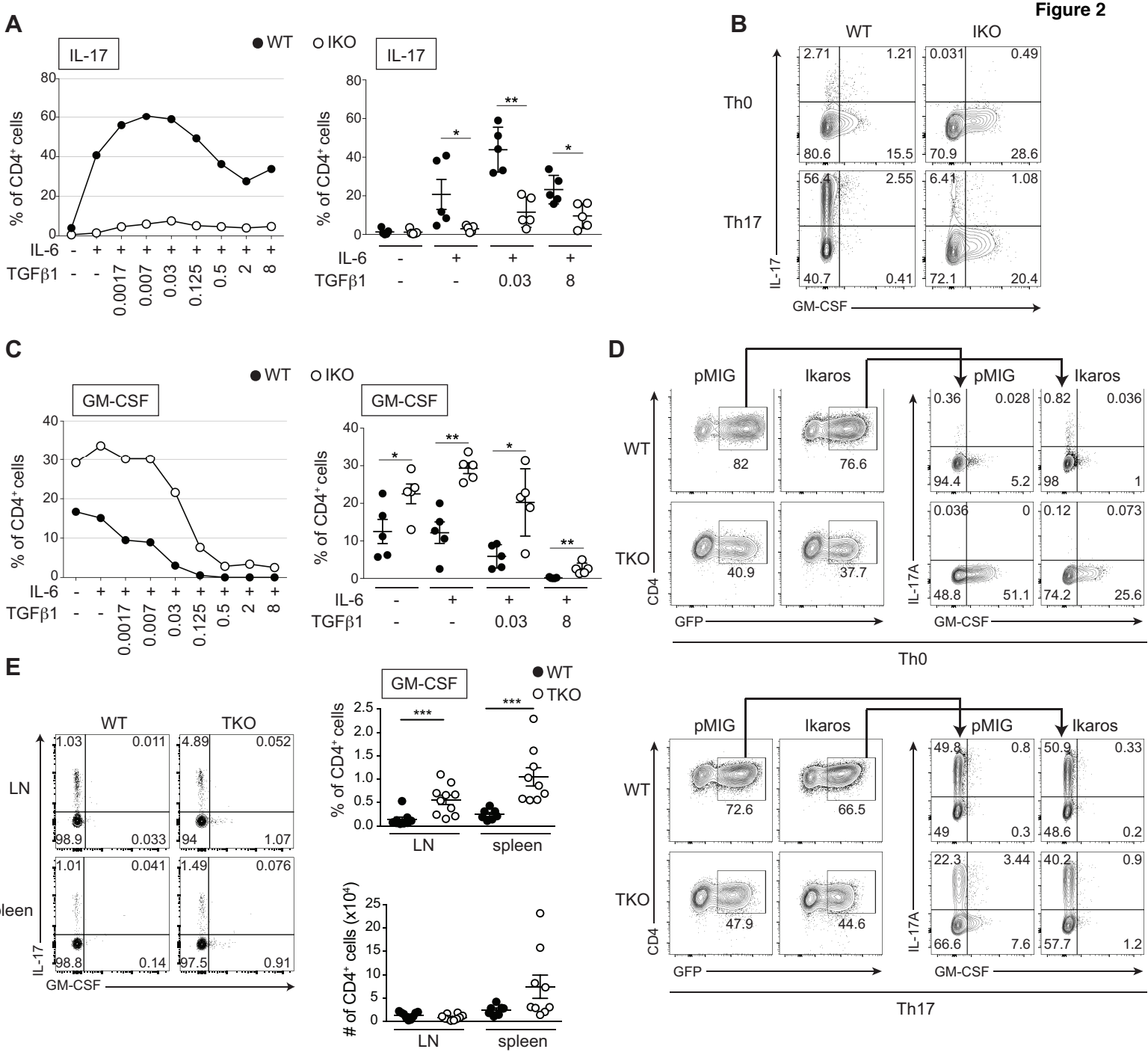
A
IL-17
WT
IKO
% of CD4+ cells
IL-6
TGFβ1
0.0017
0.007
0.03
0.125
0.5
2
8
B
WT
IKO
Th0
Th17
IL-17
GM-CSF
C
GM-CSF
D
pMIG
Ikaros
WT
TKO
CD4
GFP
IL-17A
Th0
Th17
E
LN
spleen
# of CD4+ cells (x10⁴)

Figure 3

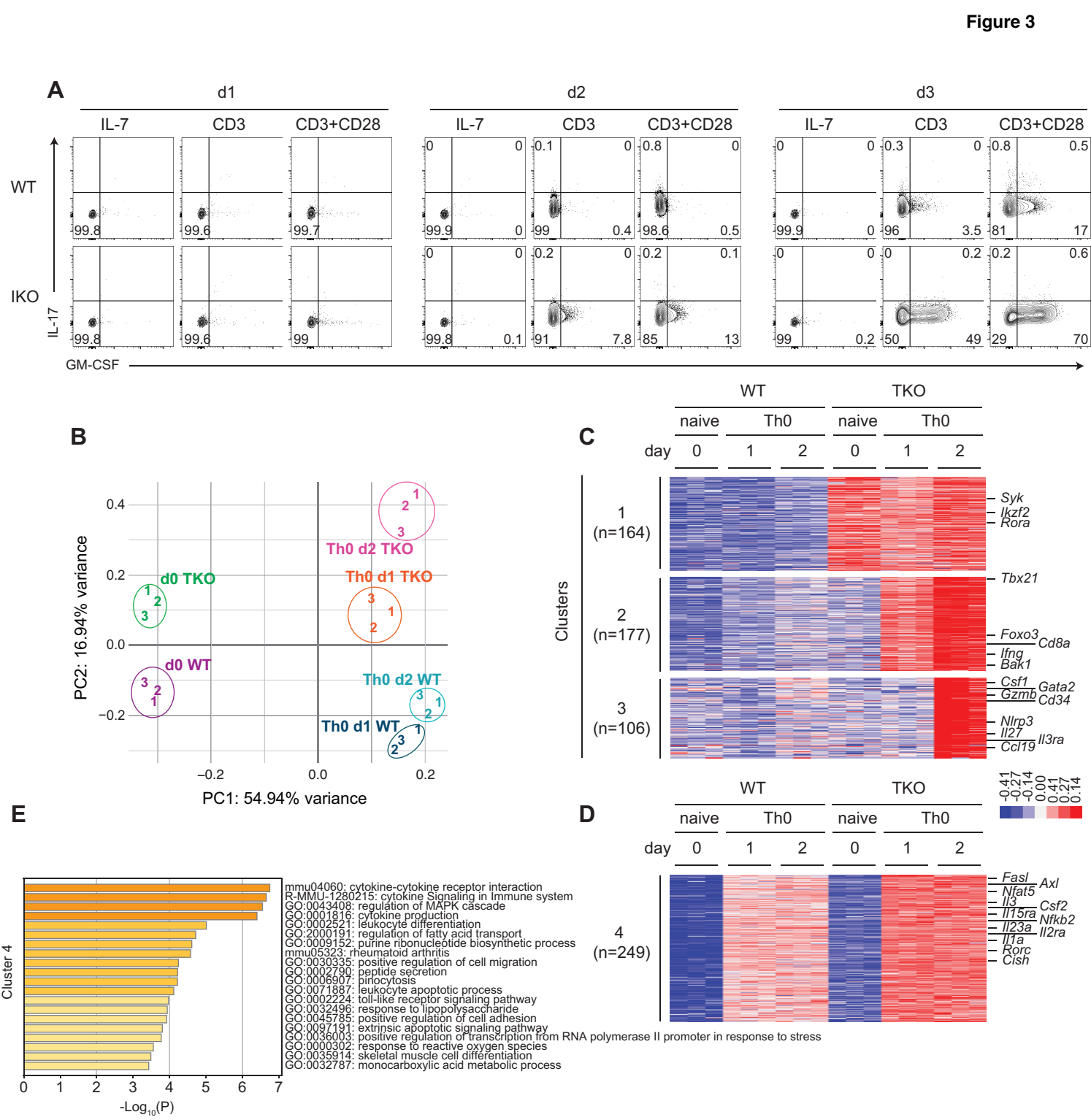
A
d1
d2
d3
IL-7
CD3
CD3+CD28
WT
IKO
IL-17
GM-CSF
B
PC2: 16.94% variance
PC1: 54.94% variance
d0 TKO
d0 WT
Th0 d2 TKO
Th0 d1 TKO
Th0 d2 WT
Th0 d1 WT
C
WT
TKO
naive
Th0
day
Clusters
1 (n=164)
2 (n=177)
3 (n=106)
Syk
Ikzf2
Rora
Tbx21
Foxo3
Cd8a
Ifng
Bak1
Csf1
Gata2
Gzmb
Cd34
Nlrp3
Il27
Il3ra
Ccl19
D
4 (n=249)
Fasl
Axl
Nfat5
Il3
Csf2
Il15ra
Nfkb2
Il23a
Il2ra
Il1a
Rorc
Cish
E
Cluster 4
-Log10(P)
mmu04060: cytokine-cytokine receptor interaction
R-MMU-1280215: cytokine Signaling in Immune system
GO:0043408: regulation of MAPK cascade
GO:0001816: cytokine production
GO:0002521: leukocyte differentiation
GO:2000191: regulation of fatty acid transport
GO:0009152: purine ribonucleotide biosynthetic process
mmu05323: rheumatoid arthritis
GO:0030335: positive regulation of cell migration
GO:0002790: peptide secretion
GO:0006907: pinocytosis
GO:0071887: leukocyte apoptotic process
GO:0002224: toll-like receptor signaling pathway
GO:0032496: response to lipopolysaccharide
GO:0045785: positive regulation of cell adhesion
GO:0097191: extrinsic apoptotic signaling pathway
GO:0036003: positive regulation of transcription from RNA polymerase II promoter in response to stress
GO:0000302: response to reactive oxygen species
GO:0035914: skeletal muscle cell differentiation
GO:0032787: monocarboxylic acid metabolic process

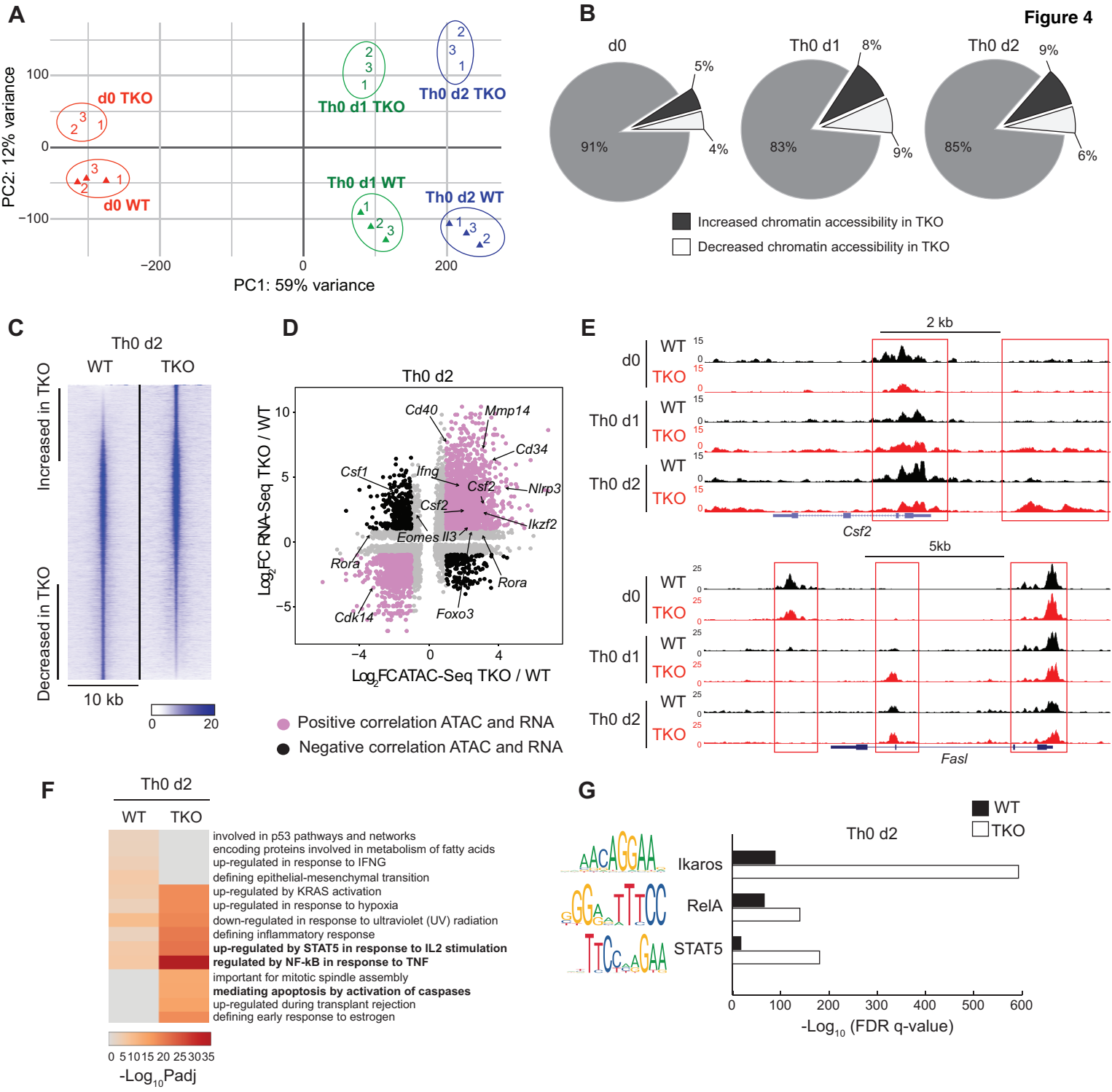
A
d0 TKO
Th0 d1 TKO
Th0 d2 TKO
d0 WT
Th0 d1 WT
Th0 d2 WT
PC2: 12% variance
PC1: 59% variance
B
d0
Th0 d1
Th0 d2
5%
91%
4%
8%
83%
9%
9%
85%
6%
Increased chromatin accessibility in TKO
Decreased chromatin accessibility in TKO
C
Th0 d2
WT
TKO
Increased in TKO
Decreased in TKO
10 kb
0
20
D
Th0 d2
Log2FC RNA-Seq TKO / WT
Log2FC ATAC-Seq TKO / WT
Cd40
Mmp14
Cd34
Csf1
Ifng
Csf2
Nlrp3
Csf2
Ikzf2
Eomes
Il3
Rora
Rora
Cdk14
Foxo3
Positive correlation ATAC and RNA
Negative correlation ATAC and RNA
E
2 kb
d0
Th0 d1
Th0 d2
WT
TKO
Csf2
5kb
Fasl
F
Th0 d2
WT
TKO
involved in p53 pathways and networks
encoding proteins involved in metabolism of fatty acids
up-regulated in response to IFNG
defining epithelial-mesenchymal transition
up-regulated by KRAS activation
up-regulated in response to hypoxia
down-regulated in response to ultraviolet (UV) radiation
defining inflammatory response
up-regulated by STAT5 in response to IL2 stimulation
regulated by NF-kB in response to TNF
important for mitotic spindle assembly
mediating apoptosis by activation of caspases
up-regulated during transplant rejection
defining early response to estrogen
-Log10Padj
G
WT
TKO
Th0 d2
Ikaros
RelA
STAT5
-Log10 (FDR q-value)

Figure 5

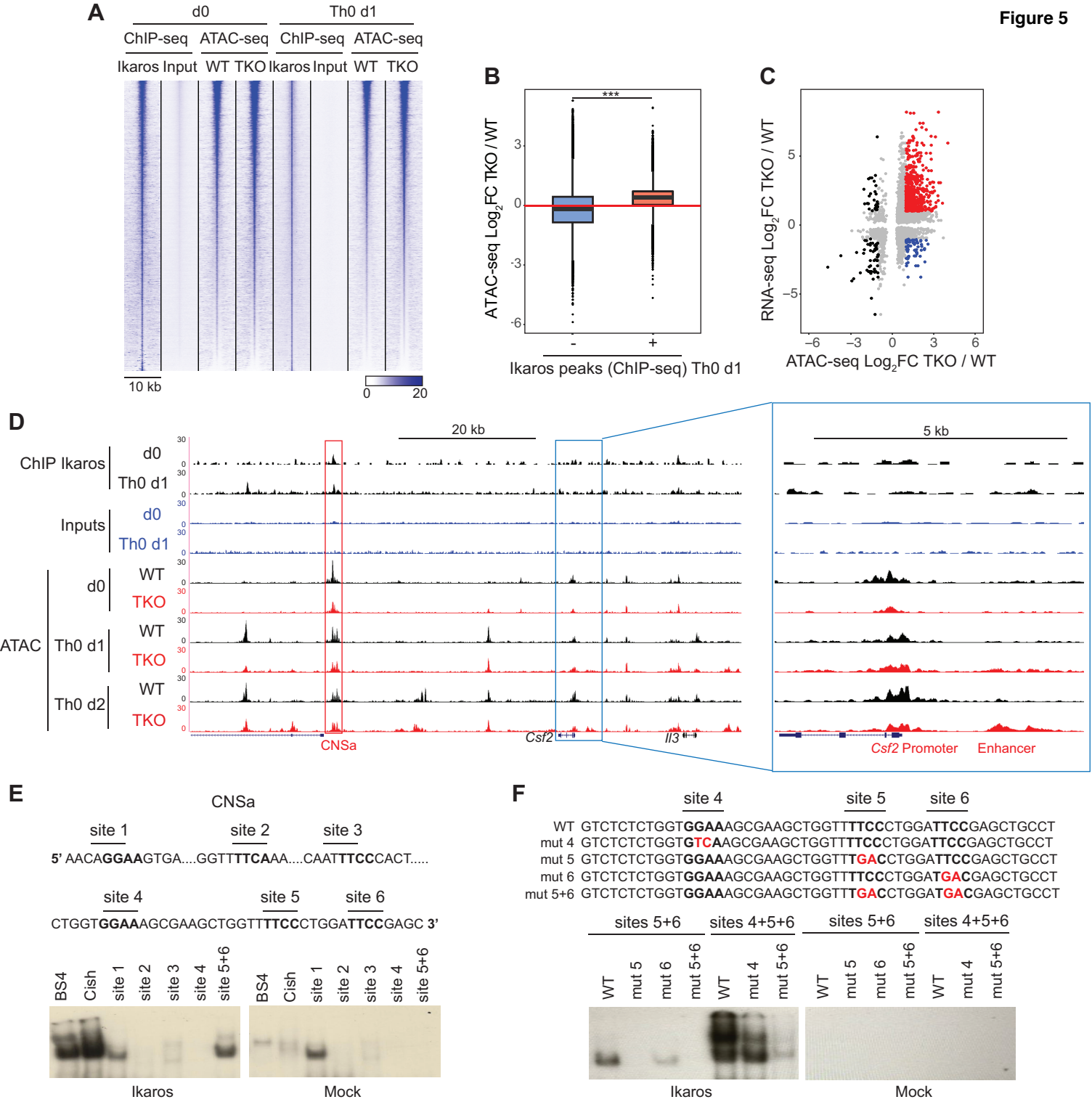
A
d0
Th0 d1
ChIP-seq
ATAC-seq
ChIP-seq
ATAC-seq
Ikaros Input WT TKO Ikaros Input WT TKO
10 kb
0 20
B
***
ATAC-seq Log2FC TKO / WT
3
0
-3
-6
-
+
Ikaros peaks (ChIP-seq) Th0 d1
C
RNA-seq Log2FC TKO / WT
5
0
−5
−6 −3 0 3 6
ATAC-seq Log2FC TKO / WT
D
20 kb
5 kb
ChIP Ikaros
d0
Th0 d1
Inputs
d0
Th0 d1
ATAC
d0
WT
TKO
Th0 d1
WT
TKO
Th0 d2
WT
TKO
CNSa
Csf2
Il3
Csf2 Promoter
Enhancer
E
CNSa
site 1
site 2
site 3
5' AACAGGAAGTGA....GGTTTTCAAA....CAATTTCCCACT.....
site 4
site 5
site 6
CTGGTGGAAAGCGAAGCTGGTTTTCCCTGGATTCCGAGC 3'
BS4
Cish
site 1
site 2
site 3
site 4
site 5+6
Ikaros
Mock
F
site 4
site 5
site 6
WT GTCTCTCTGGTGGAAAGCGAAGCTGGTTTTCCCTGGATTCCGAGCTGCCT
mut 4 GTCTCTCTGGTGTCAAGCGAAGCTGGTTTTCCCTGGATTCCGAGCTGCCT
mut 5 GTCTCTCTGGTGGAAAGCGAAGCTGGTTTGACCTGGATTCCGAGCTGCCT
mut 6 GTCTCTCTGGTGGAAAGCGAAGCTGGTTTTCCCTGGATGACGAGCTGCCT
mut 5+6 GTCTCTCTGGTGGAAAGCGAAGCTGGTTTGACCTGGATGACGAGCTGCCT
sites 5+6
sites 4+5+6
sites 5+6
sites 4+5+6
WT
mut 5
mut 6
mut 5+6
WT
mut 4
mut 5+6
WT
mut 5
mut 6
mut 5+6
WT
mut 4
mut 5+6
Ikaros
Mock

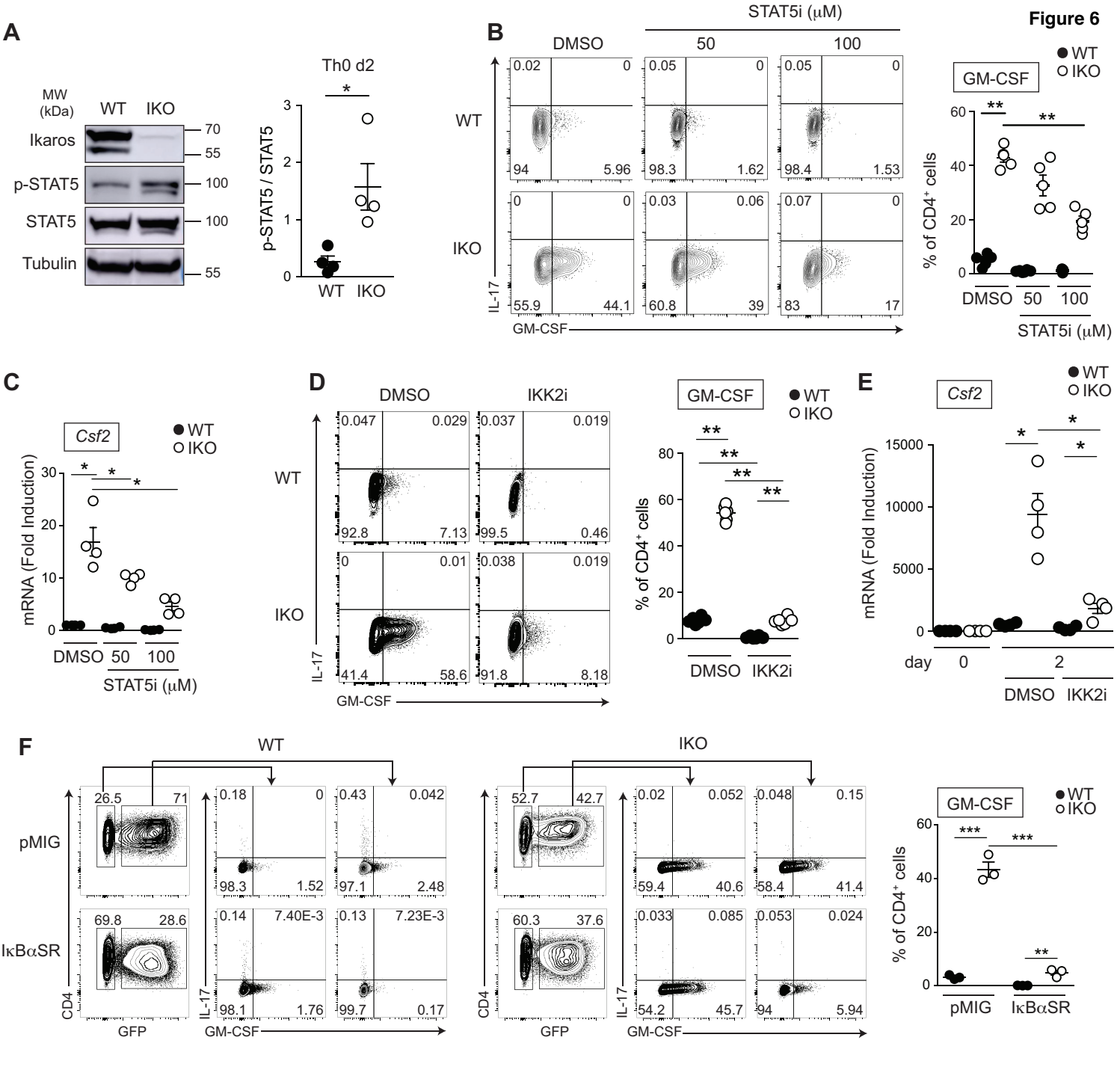
A
MW (kDa)
WT
IKO
Ikaros
p-STAT5
STAT5
Tubulin
70
55
100
100
55
Th0 d2
p-STAT5 / STAT5
WT
IKO
B
STAT5i (μM)
DMSO
50
100
WT
IKO
IL-17
GM-CSF
GM-CSF
% of CD4+ cells
DMSO
50
100
STAT5i (μM)
C
Csf2
mRNA (Fold Induction)
DMSO
50
100
STAT5i (μM)
D
DMSO
IKK2i
WT
IKO
IL-17
GM-CSF
GM-CSF
% of CD4+ cells
DMSO
IKK2i
E
Csf2
mRNA (Fold Induction)
day
0
2
DMSO
IKK2i
F
WT
IKO
pMIG
IκBαSR
CD4
GFP
IL-17
GM-CSF
GM-CSF
% of CD4+ cells
pMIG
IκBαSR

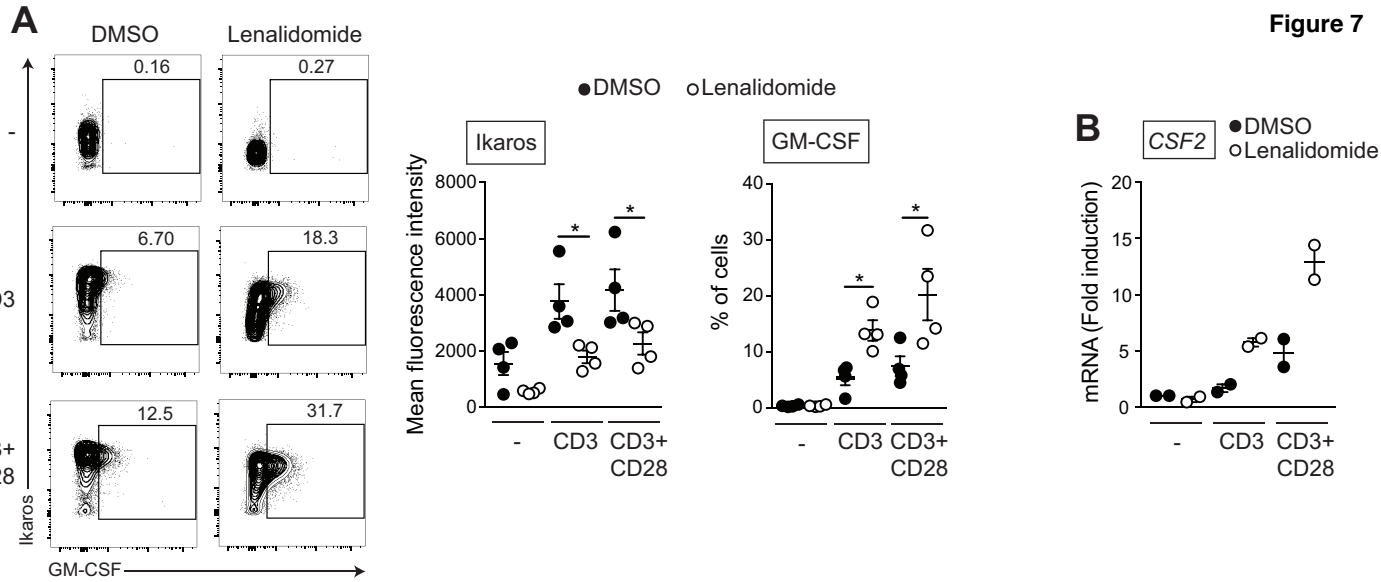
A
DMSO
Lenalidomide
0.16
0.27
6.70
18.3
12.5
31.7
-
CD3
CD3+
CD28
Ikaros
GM-CSF
DMSO
Lenalidomide
Ikaros
Mean fluorescence intensity
8000
6000
4000
2000
0
*
*
-
CD3
CD3+
CD28
GM-CSF
% of cells
40
30
20
10
0
*
*
-
CD3
CD3+
CD28
B
CSF2
DMSO
Lenalidomide
mRNA (Fold induction)
20
15
10
5
0
-
CD3
CD3+
CD28

PNAS
www.pnas.org

Supplementary Information for

CD4$^+$ T cells require Ikaros to inhibit their differentiation towards a pathogenic cell fate

Chiara Bernardi, Gaëtan Maurer, Tao Ye, Patricia Marchal, Bernard Jost, Manuela Wissler, Ulrich Maurer, Philippe Kastner*, Susan Chan* and Céline Charvet*

***Correspondence:**
Céline Charvet (charvetc@igbmc.fr)
Philippe Kastner and Susan Chan (scpk@igbmc.fr)
IGBMC, 1 rue Laurent Fries, BP 10142, 67404 Illkirch CEDEX, France

This PDF file includes:

SUPPLEMENTARY MATERIALS AND METHODS

DNA constructs

The murine IκBα super repressor (IκBαSR) contains mutations preventing its phosphorylation and degradation and has been described to inhibit the nuclear translocation of NFκB as it *(1), (2)* into the pMIG vector, upstream of the IRES-GFP sequence, using the restriction enzyme EcoRI. The murine Ikaros was subcloned into the pMIG vector, upstream of the IRES-GFP sequence using the restriction enzymes XhoI and EcoRI.

Retroviral infections

Primary $CD4^+$ T cell infection was performed as described with minor changes *(3)*. For virus production, Platinum-E packaging cells (plat-E) were transfected either with pMIG, Ikaros (Ik-1)/pMIG or IκBαSR/pMIG using lipofectamine 2000 (Invitrogen) in a 10-cm culture dish. One day later, the medium was replaced by 6 ml of IMDM 10% FCS and the retroviral supernatant was harvested after 24 h and filtered in a 0.45 µm filter. This step was repeated for a 2nd harvest and both harvests were frozen at -80°C. For retroviral infection, naive $CD4^+$ T cells were sorted and directly cultured in Th0 (no cytokines added) or Th17 (with IL-6 and TGFβ1) conditions in a 96-well NUNC plate at 4 x 10^4 cells/well in 200 µl of IMDM 10% FCS. One day later, the medium was replaced by the retroviral supernatant containing polybrene (8 µg/ml), QVD-Oph (20 µM), in Th0 or Th17 conditions. Cells were centrifuged 1h at 2000 rpm RT and incubated at 37°C for 3h. This step was then repeated once the same day, the medium was then exchanged with IMDM 10% FCS and QVD-OPh (20 µM) in Th0 or Th17 conditions and cells were cultured at 37°C. Two days after the infection, cells were stimulated with PMA, ionomycin (0.5 µg/ml each) and GolgiPlug™ (1/1000) for 2h, stained with Zombie Aqua™ fixable viability dye (Biolegend), anti-CD4 Ab, fixed and permeabilized using the BD Cytofix/Cytoperm kit, and stained intracellularly with GM-CSF and IL-17. Cells were then analyzed on the cytometer LSRII (BD Biosciences).

Electrophoretic Mobility Shift Assay (EMSA)

EMSA was performed as described *(4)*. Cos cells were transfected with the vector pTL2 expressing the murine Ikaros-1 isoform or not (mock) and the nuclear extracts were used with the probes indicated in the supplemental table 2.

T cell division

$CD4^+$ naive T cells (2-3 $x10^6$) from LN were sorted, resuspended in 900 µl of IMDM 10% FCS and labelled with CFSE (10 µM) by adding 100 µl of a 100 µM CFSE stock with gentle vortex for 10 min at 37°C. CFSE-labelled cells were then washed 3 times with IMDM 10 % FCS and cultured ($4x10^4$ cells / well) in Th0 or Th17 conditions as described above, with QVD-Oph (20 µM). When indicated, at day 3, cells were stimulated with PMA plus ionomycin (0.5 µg/ml each) and GolgiPlug™ (1/1000) for 2h for cytokine expression. Cells were then first stained with a Zombie Aqua™ fixable viability dye (Biolegend) according to the manufacturer's protocol and with an anti-CD4 Ab, fixed and permeabilized using the Foxp3 Fixation/Permeabilization kit (eBiosciences), and stained with anti-IL-17, anti-GM-CSF. CFSE intensity and intracellular cytokines expression were analyzed in live cells, using the cytometer LSRII (BD Biosciences).

RT-qPCR

For murine cells, total RNA was extracted using the RNeasy Plus microkit (QIAGEN) according to the manufacturer's protocol. For human cells, PBLs ($2x10^5$ / well) were activated or not with plate bound anti-CD3 ± anti-CD28 Abs (10 µg/ml each) with Lenalidomide (10 µM) or DMSO as a control. After 2 days, total RNA was extracted using the Nucleospin RNA kit (Macherey-Nagel) according to the manufacturer's protocol. In both cases, cDNAs were obtained by using the Superscript IV (Invitrogen) and quantitative PCR was performed using the FastStart SybrGreen system (Roche) with the primers listed in the supplemental table 1. mRNA expression of the genes of interest was normalized to *L32* mRNA and -fold induction of each condition was calculated.

Western blot

Cells were lysed in 30 µl of lysis buffer *(5)* supplemented with complete protease inhibitor cocktail (11873580001, Roche), phosphatase inhibitor cocktail 3 (P0044, Sigma), SDS 0.1% and Bitnuclease (4 U/µl; B16002, Benzonase® alternative, Biotool) for 15 min on ice. After centrifugation at 13, 000 rpm at 4°C, the supernatant was harvested and the proteins were separated on a 10% SDS-PAGE and transferred on a nitrocellulose membrane. For STAT5, cells were lysed as above without the addition of SDS and Bitnuclease. Ikaros expression was analyzed using the anti-Ikaros (A3) Ab. Anti-phosphoY694-STAT5 (D47E7) and anti-STAT5 (D206Y) Rabbit mAbs were from Cell Signaling Technologies. Anti-tubulin α (YL1/2) and Anti-β-actin (AC-15) Abs were from Abcam and Sigma-Aldrich, respectively.

Microarray analysis

Purified naive $CD4^+$ T cells (0.5×10^6 / well) from spleen were activated on a 48-well plate, pretreated with Goat anti-Hamster IgG and coated with anti-CD3 (2C11; 1 µg/ml) and anti-CD28 (37.51; 0.25µg/ml) Abs, in the presence of mIL-6 (20 ng/ml), hTGFβ1 (1 ng/ml) and neutralizing anti-IL-4 and anti-IFNγ Abs (2 µg/ml each). A transcriptome analysis was performed using GeneChip Mouse Gene 2.0ST arrays (Affymetrix) with cells cultured for 1 and 2 days as well as with naive $CD4^+$ T cells (day 0). Raw data were analyzed using the software Affymetrix version 1.4.1 and the Robust Multiarray Average (RMA) method. K-means clustering was performed using Cluster 3.0, using genes that were differentially expressed (Log_2 FC > 0.5, corresponding to a FC > 1.42) between WT and TKO cells at any of the timepoints analyzed, or between two timepoints in either WT or TKO cells. Principal component analysis (PCA) were performed using the prcomp function in R software and the figure was performed with the ggplot 2 package. Genes with several probes on the microarray were selected and only probes with the highest FC TKO/WT value were retained. GSEA was then performed using the GSEA 2.0 software after selecting differentially regulated genes in TKO vs. WT T cells by the FCROS method with an error set at 10% *(6)*.

Chromatin ImmunoPrecipitation (ChIP)

The ChIP protocol was performed according to different protocols with some changes *(7, 8)*. Briefly, WT naive $CD4^+$ T cells (10×10^6) and activated for 1 day (9×10^6) were washed in PBS and cross-linked in PBS/0.5%BSA/1% ultrapure formaldehyde (Electron Microscopy Sciences) for 10 min at 37°C. Glycine (125 mM) was added as a quenching agent and cells were then washed 2 times with 3 ml of cold PBS and permeabilized in 3 ml of cell lysis buffer (0.25%, Triton-X100, 10 mM EDTA, 0.5 mM EGTA, 10 mM Hepes pH 6.5 and complete proteases inhibitors (Roche)) on ice for 10 min. After centrifugation at 2000 rpm for 10 min, the nuclei pellets were resuspended in 300 µl of SDS lysis buffer (1% SDS, 10mM EDTA, 50 mM Tris pH 8.0 and complete proteases inhibitors). 700 µl of ChIP dilution buffer (0.01% SDS, 1.1% Triton X-100, 1.2 mM EDTA, 16.7 mM Tris-HCl pH8.1, 167 mM NaCl containing complete proteases inhibitors) were then added and samples were sonicated in a 1 ml round-bottom glass tubes (Covaris®) using the Covaris E220 sonicator (Peak incident power 100, Duty factor 50, 200 cycles/burst) for 10 min to generate DNA fragment between 150-300 bp. Of note, the expression of Ikaros was controlled before and after sonication and remained similar. After sonication, the samples were centrifuged at 14, 000 rpm for 10 min. The supernatant containing the chromatin was pre-cleared with 25 µl of dynabeads

magnetic prot A for 1h at 4°C. 2.5 x 10^5 cell equivalent of the sample was kept as the input and the pre-cleared chromatin was then incubated overnight with anti-Ikaros (1/100). The next day, 25 µl of dynabeads magnetic prot A were added for 5h. The prot-DNA complexes bound to the Ab and the beads were then washed 1x with low-salt buffer (0,1% SDS, 1% TTX, 2 mM EDTA, 20 mM Tris-Hcl pH8.1, 150 mM NaCl and complete protease inhibitors), 1x with high-salt buffer (0,1% SDS, 1% TTX, 2mM EDTA, 20mM Tris-Hcl pH8.1, 500mM NaCl and complete proteases inhibitors), 2x with LiCl buffer (250mM LiCl, 1% IGEPAL-CA630, 1% deoxycholic acid, 1mM EDTA, 10mM Tris pH8.1 and complete proteases inhibitors) and 1x with TE **(**50 mM Tris pH 8.0, 10 mM EDTA). Samples were then eluted by adding 150 µl of Elution buffer (50mM Tris pH 8.0, 10mM EDTA, 1% SDS) and incubate at 65°C for 10 min with shaking. This step was repeated twice. The reverse crosslink was performed by the ChIP and input samples with NaCl (200 mM) at 65°C ON. Next morning, proteinase K (80 µg) was added for 1 h at 45°C and DNA was purified using phenol/chloroform and phase lock tubes^{TM} (Invitrogen).

ChIP-sequencing and analysis

Libraries were performed using the MicroPlex Library Preparation kit (#C05010014, Diagenode), following Manufacturer's instructions. The library was sequenced on Illumina 4000 sequencer as Single-Read 50 base reads following Illumina's instructions. Image analysis and base calling were performed using RTA 2.7.7 and bcl2fastq 2.17.1.14. Adapter dimer reads were removed using Dimer Remover (https://sourceforge.net/projects/dimerremover/). Alignment was performed to mm10 mouse genome using Bowtie 1.0.0 *(9)* with the following arguments: -m 1 --strata --best -y -S -l 40. Peak calling was performed using MACS2 v2.1.1.20160309 with default parameters *(10)*. The Th0 d1 input was used as the control for peak-calling for the d0 and Th0 d1 conditions. Peaks were annotated with Homer software *(11)* using Ensembl release 94 gene annotation. In order to find the common peaks bound by Ikaros in the d0 and Th0 d1 conditions, the Ikaros peaks at d0 were intersected with the Th0 d1 Ikaros peaks with the Bedtools program. Data were visualized using UCSC Genome Browser with default parameters *(12)* and seqMINER_1.3.3g (normalized to 20x10^6 reads randomly selected and ordered by read coverage) *(13)*. Identification of the ATAC-seq peaks bound by Ikaros at d1 was performed by intersecting all ATAC-seq regions at d1 (present in WT or/and in TKO) with all Ikaros peaks at d1 using the Bedtools program.

Assay for Transposase-Accessible Chromatin (ATAC)

Naive WT and TKO CD4$^+$ T cells were sorted on a FACS ARIA^{TM} FUSION (BD Biosciences) cell sorter. Naive CD4$^+$ WT and TKO T cells (5 x 10^4) were directly used for the ATAC-seq protocol for the day 0 condition, while the remaining naive WT and TKO CD4$^+$ T cells were activated with coated anti-CD3, anti-CD28 Abs (2 µg/ml) in the presence of neutralizing anti-IL-4 and anti-IFNγ Abs (10 µg/ml). At day 1 and 2, live WT and TKO cells (5 x 10^4 DAPI$^-$ cells) were sorted on a FACS ARIA^{TM} FUSION (BD Biosciences) and used for the ATAC-seq protocol. Three independent experiments were performed. The ATAC-seq protocol has been performed as previously described (Buenrostro et al., 2013). Briefly, cells were lysed with cold lysis buffer (10 mM Tris-HCl, pH7.4, 10 mM NaCl, 3 mM MgCl2, 0.1 % (v/v) Igepal CA-630) and nuclei were pelleted 10 min at 500g. Nuclei were incubated with the transpose reaction mix for 30 min at 37 °C. Immediately following transposition, the fragmented DNA was purified using Qiagen MinElute PCR Purification Kit and eluted in 10 µL. The transposed DNA fragments was amplified by PCR for 5 cycles. To determine the appropriate number of PCR cycles to add for each condition, a qPCR was performed. The appropriate number of cycles (6-9 cycles) was then added to each sample. PCR fragments were purified two times with SPRIselect (Beckman Coulter, #B23317) and the quality of the purified libraries was analyzed using a Bioanalyzer High-Sensitivity DNA Analysis kit (Agilent).

ATAC-sequencing and analysis

The libraries were sequenced on Illumina Hiseq 4000 sequencer as Paired-End 100 base reads following Illumina's instructions. Image analysis and base calling were performed using RTA 2.7.7 and bcl2fastq 2.17.1.14. Data analysis was performed using the Encode ATAC-seq pipeline v1.4.2. Adapter sequences were removed and low-quality ends were trimmed. Sequence alignment was performed into the mm10 assembly of Mus musculus genome using Bowtie2 (version 2.2.6) choosing the zero multi-mapping option. Mitochondrial reads were removed. The Peak calling was performed using MACS2 v2.1.1.20160309 *(10)*. Finally, the conserved overlap peaks were used for the analysis. Peaks from different conditions were merged to form a consensus peak set. The peaks were annotated using annotatePeaks.pl script in Homer program *(11)*and with Ensembl 94 database. The read coverage for each sample was calculated with multicov function from bedtools program (v2.26.0). Comparisons of interest were performed using the test for differential expression, proposed by Love et al. and implemented in the Bioconductor package DESeq2 version 1.16.1 *(14)*. Motif research for selected peaks specifically significant in the TKO or WT conditions (log_2FC TKO/WT > 2 or < -2 with a padj <0.01) was

performed at the MEME website using the AME software *(15)* and the ones of interest were represented by bar graph using Illustrator. For the PCA analysis, read counts have been normalized across samples with the median-of-ratios method proposed in DESeq2 package. Principal Component Analysis was computed on variance stabilizing transformed data. ATAC-seq data were represented by Volcano plots using ggplot2 package (R). Data were visualized using UCSC Genome Browser *(12)*, seqMINER_1.3.3g (normalized to $20x10^6$ reads randomly selected from the pooled data and ordered by read coverage) *(13)*. Pathway analysis were performed at the GSEA website using Hallmark gene set collection in the MSig Datatabase and represented by heatmap using the plotly package (R v3.6.2) *(16-18)*.

RNA-sequencing and analysis

At day 0, naive $CD4^+$ WT and TKO T cells (4-6 x 10^6) were sorted on a FACS ARIA™ FUSION (BD Biosciences). Naive $CD4^+$ WT and TKO T cells (1 x 10^6) were used directly and the remaining cells were activated with coated anti-CD3, anti-CD28, and anti-IL-4 and anti-IFNγ Abs. At day 1 and 2, live WT and TKO cells (1-2 x 10^5 $DAPI^-$ cells) were sorted on a FACS ARIA™ FUSION (BD Biosciences). Total RNA was extracted from using the RNeasy Plus Micro kit (Qiagen) according to the manufacturer's instructions. Libraries were prepared with the Clontech SMART-seq v4 Ultra Low Input RNA Kit for Sequencing and sequenced with HiSeq 4000 (Illumina) with single-end 50 bp read length.

The RNA analysis was done using the GenomEast RNA-seq pipeline version 1.2.2. Reads were preprocessed in order to remove adapters, polyA and low-quality sequences (Phred quality score below 20). After this preprocessing, reads shorter than 40 bases were discarded for further analysis. These preprocessing steps were performed using Cutadapt version 1.10 *(19)*. Reads were mapped into the mm10 assembly of Mus musculus genome using STAR version 2.5.3a *(20)*. The reads were aligned across exonic, intronic and intergenic genomic region using annotations from Ensembl 94. Gene expression quantification was performed from uniquely aligned reads using Htseq-count version 0.6.1p1, with annotations from Ensembl version 94 and "union" mode *(21)*. Only non-ambiguously assigned reads have been retained for further analyses. In order to make these counts comparable between samples, read counts have been normalized across samples with the median-of-ratios method proposed by Anders and Huber *(22)*. Comparisons of interest were performed using the test for differential expression, proposed by Love et al. and implemented in the Bioconductor package DESeq2 version 1.16.1 *(14)*. Heatmaps of differentially expressed genes (K-means) were created using Cluster 3 and Java Treeview softwares. Selected genes that were differentially expressed (data normalized and divided

by median of transcripts length in kb with a value ≥ 50 and FC ≥ 3.5) between WT and TKO cells at any of the timepoints analyzed, or between two timepoints in either WT or TKO cells. For the GSEA, up- and down-regulated genes in the TKO conditions were selected (pvalue ≤ 0.05 and log_2FC ≥ 2 or ≤ -2). Pathways analysis were performed using the Metascape website *(23)*. For the PCA analysis, read counts have been normalized across samples with the median-of-ratios method proposed in DESeq2 package. Principal Component Analysis was computed on regularized logarithm transformed data. The RNAseq result was integrated into the ATAC-seq data with the same Ensembl gene ID and the data were visualized using ggplot2 (R).

SUPPLEMENTARY FIGURE LEGENDS

Fig. S1. Differentially expressed genes in WT and TKO T cells in Th17 conditions.
(A) Western blot showing the T-cell specific deletion of Ikaros in splenic $CD4^+$ and $CD8^+$ cells vs. $B220^+$ cells in TKO mice. **(B)** Clusters of upregulated genes in WT and TKO $CD4^+$ T cells cultured in Th17 conditions (K-means clustering) **(C)** Clusters of upregulated genes in WT and TKO $CD4^+$ T cells cultured in Th17 conditions (K-means clustering). **(D)** RT-qPCR analysis of *Il17 and Rorc* mRNA expression in freshly isolated naive $CD4^+$ T cells (d0) or after culture in Th17 conditions with QVD-OPh for 1 and 2 days (n=4; mean ± SEM). **(E)** Heat maps of GO term enrichment of genes in cluster 18 shown in B.

Fig. S2. Gene set enrichment analysis of pathogenic genes in TKO cells.
(A) GSEA enrichment plots of genes enriched in pTh17 (left) or cTh17 cells (right) among genes up- or down-regulated by Ikaros at d2 in Th17 conditions. Gene sets correspond to 106 genes enriched in pTh17 cells and 143 genes enriched in cTh17 cells *(24)*. **(B)** GSEA enrichment plots of genes enriched in Th-GM cells among genes up- or down-regulated by Ikaros at d1 (left) and d2 (right) in Th17 conditions. Gene sets correspond to 210 genes enriched in Th-GM cells *(25)*. **(C)** GSEA enrichment plots of genes in Th17 cells infiltrating the central nervous system during EAE, among genes up- or down-regulated by Ikaros at d1 (left) and d2 (right) in Th17 conditions. Gene sets correspond to 1041 genes either upregulated (Log2FC ≥ 2) or downregulated (Log2FC ≤ -2) in Th17 cells infiltrating the central nervous system (CNS) during EAE compared to the ileum (GSE127768) *(26)*. NES, normalized enrichment score; FDR, false discovery rate.

Fig. S3. Ikaros loss leads to decreased IL-17 and Foxp3 and increased IFNγ and GM-CSF levels.
(A) Western blot of Ikaros expression in WT or IKO splenic $CD19^+$ or $CD4^+$ cells of tamoxifen-treated mice. β-Actin was used as a loading control. **(B)** Contour plots showing naive $CD4^+$ T cells ($CD4^+CD8^-CD44^{lo/-}CD25^-TCR^{\gamma\delta-}NK1.1^-$) from peripheral and mesenteric LN of tamoxifen-treated WT and IKO mice. **(C and D)** Proportions of $Foxp3^+CD4^+$ (C; left) or $IFN\gamma^+CD4^+$ cells (D; left) and statistical analysis of the proportion of WT and IKO $Foxp3^+CD4^+$ cells (C; right) or $IFN\gamma^+CD4^+$ (D; right) cells from 3d cultures of WT and IKO cells (from tamoxifen-treated mice), cultured in Th17 conditions with different amounts of TGFβ1 plus constant IL-6. (n=5; mean ± SEM). Statistical significance was analyzed by a Mann-Whitney test (*p ≤0.05, **p ≤ 0.01). **(E-H)** Representative graphs showing the

intracellular expression of IFNγ (E), IL-17 (F), Foxp3 (G), and GM-CSF (H) in WT and IKO $CD4^+$ T cells cultured for 3 days with different amounts of TGFβ1 plus constant IL-6 with QVD-Oph, and with or without neutralizing anti-IFNγ and anti-IL-4 Abs (n=4).

Fig. S4. Ikaros loss leads to an increased expression of FasL that is responsible for apoptosis but not GM-CSF production.

(A) Left: representative contour plots of Annexin V and PI staining on WT and IKO $CD4^+$ cells cultured for 2d in Th17 conditions with or without QVD-OPh. Right: proportions of WT and IKO Annexin V^+ cells. Each dot indicates one mouse (n=4-5; mean ± SEM). **(B)** RT-qPCR analysis of *Fasl* mRNA expression in WT and IKO LN naive $CD4^+$ cells after harvest (d0), or cultured in Th0 or Th17 conditions with QVD-OPh (d1 and 2). *Fasl* mRNA expression is represented as -fold induction with respect to the d0 WT sample. **(C)** Left: representative contour plots showing membrane FasL expression at d3 in WT and IKO cells cultured in Th0 conditions. Right: proportions of WT and IKO $FasL^+$ $CD4^+$ T cells (n=4; mean ± SEM). **(D)** Left: representative contour plot showing Annexin V and PI staining of WT and IKO $CD4^+$ T cells cultured for 2 days in Th0 condition with a neutralizing anti-FasL Ab or an isotype control. Right: proportions of WT and IKO annexin V^+ $CD4^+$ T cells at d2 (n=4; mean ± SEM). **(E)** Left: percentage of $GM\text{-}CSF^+$ and $IL\text{-}17^+$ cells among live WT or IKO $CD4^+$ cells cultured for 3 days in Th0 conditions with a neutralizing anti-FasL Ab or an isotype control. Right: proportion of WT and IKO $GM\text{-}CSF^+$ $CD4^+$ T cells (n=4; mean ± SEM). N indicates the number of independent experiments. Statistical significance was analyzed by a Mann-Whitney test (*$p \leq 0.05$, **$p \leq 0.01$).

Fig. S5. GM-CSF expression and IL-17 loss of expression directly correlate with *Ikzf1* deletion.

(A) Left: representative contour plots showing GM-CSF and Ikaros expression in WT and IKO cells treated with ethanol (EtOH)- or 4-hydroxytamoxifen (4-OHT) *in vitro* for 1-3 days in the presence of QVD-OPh, and analyzed at the indicated time point. Right: proportion at d3 of $Ikaros^+$ $GM\text{-}CSF^+$ cells from 4-OHT-treated WT cultures, or $Ikaros^-$ $GM\text{-}CSF^+$ cells from 4-OHT-treated IKO cultures, performed as in A (n=4; mean ± SEM). **(B)** Left: representative contour plot showing IL-17 and Ikaros expression in EtOH- and 4-OHT-treated live WT and IKO cells cultured as in A. Right: proportions at d2 and d3 of $Ikaros^+$ $IL\text{-}17^+$ cells from 4-OHT-treated WT cultures, and $Ikaros^-$ $IL\text{-}17^+$ cells from 4-OHT-treated IKO cultures, performed under in Th17 conditions (n=4; mean ± SEM). Statistical significance was analyzed by a Mann-Whitney test (*$p \leq 0.05$).

Fig. S6. Analysis of mature T cells in TKO mice.

All mice were 5-8 weeks old. **(A)** Total cell number in WT and TKO LN and spleen (n=7). **(B)** Left: $CD4^+$ and $CD8^+$ T cell numbers in LN and spleen from WT and TKO mice. Right: proportion of $CD4^+$ and $CD8^+$ T cells in WT and TKO LN and spleen (n=6). **(C)** Left: $CD19^+$ cell count in WT and TKO LN and spleen. Right: corresponding percentage of $CD19^+$ cells (n=5). **(D)** Representative contour plots of naive and effector $CD4^+$ T cells in LN from WT and TKO mice. **(E)** Left: naive $CD4^+$ T cell counts in LN and spleen. Right: percentage of naive cells among $CD4^+TCR\alpha\beta^+$ T cells (n=4). **(F)** Left: effector $CD4^+$ T cell counts in LN and spleens. Right: percentage of effector cells among $CD4^+TCR\alpha\beta^+$ cells (n=4). **(G)** Relative expression levels of IL-7Rα in WT and TKO naive $CD4^+$ T cells from LN and spleen (n=4). For a given organ (LN or spleen), the values for each mouse analyzed in a given experiment were normalized to the mean expression value for the WT samples analyzed in that experiment. All graphs are represented as mean ± SEM. Each circle indicates one mouse. n indicates the number of independent experiments. Statistical significance was analyzed by a Mann-Whitney test (*$p \leq 0.05$, **$p \leq 0.01$, ***$p \leq 0.001$ and ****$p \leq 0.0001$).

Fig. S7. Ikaros loss leads to an increase of GM-CSF expression in $CD4^+$ T cells, but not $CD8^+$ T cells, ex vivo.

(A) Left panel: Representative analysis of GM-CSF- and CD8-expressing cells in WT and TKO T cells in LN and spleen. Middle panel: percentage of GM-CSF^+ cells among $CD8^+$ T cells from peripheral and/or mesenteric LN (n=9-10) or spleen (n=7-9) from WT and TKO mice. Right panel: cell counts of GM-CSF^+ cells among WT and TKO $CD8^+$ T cells from peripheral and/or mesenteric LN (n=9-10) or spleen (n=7-9) of WT and TKO mice (mean ± SEM). **(B)** Left panel: percentage of IL-17^+ cells among $CD4^+$ T cells from peripheral and/or mesenteric LN (n=9-10) or spleen (n=7-9) from WT and TKO mice. Right panel: cell counts of IL-17^+ cells among WT and TKO $CD4^+$ T cells from peripheral and/or mesenteric LN (n=9-10) or spleen (n=7-9) of WT and TKO mice (mean ± SEM). Statistical significance was analyzed by a Mann-Whitney test (**$p \leq 0.01$).

Fig. S8. Differentially expressed genes in WT and TKO T cells in Th0 conditions.

(A) Proportion of WT and IKO GM-CSF^+ $CD4^+$ T cells after 2 and 3 days of culture with anti-CD3 ± anti-CD28 Abs, related to Fig. 3A (n=4; mean ± SEM). Statistical significance was analyzed by a Mann-Whitney test (*$p \leq 0.05$)**. (B)** Clusters of upregulated genes in WT and TKO $CD4^+$ T cells cultured in Th0 conditions (K-means clustering). **(C)** Clusters of

downregulated genes in WT and TKO CD4$^+$ T cells cultured in Th0 conditions (K-means clustering).

Fig. S9. Enriched pathways in clusters 1-3. Metascape analysis of GO term enrichment of genes in clusters 1-3 from RNA-seq.

Fig. S10. CD4$^+$ T cells require Ikaros to proliferate.

(A) Left: Representative histogram of CFSE dilution and proliferative index of WT and IKO CD4$^+$ T cells at d3 in Th0 conditions (n=6; mean ± SEM). Right: Representative histogram of CFSE dilution and proliferative index of WT and IKO CD4$^+$ T cells at d3 in Th17 conditions (n=4; mean ± SEM). **(B)** Left: representative dot plot showing CFSE dilution and GM-CSF expression in WT and IKO CD4$^+$ T cells in Th0 (upper panel) or Th17 conditions (lower panel) for 3d. Right: percentage of GM-CSF$^+$ cells among WT and IKO CD4$^+$ T cells, in Th0 (upper panels; n=5; mean ± SEM) or Th17 conditions (lower panel; (n=4; mean ± SEM), in each division peak. N=number of independent experiments. Statistical significance was analyzed by a Mann-Whitney test (*p ≤ 0.05, **p ≤ 0.01). **(C)** Left: representative dot plot showing CFSE dilution and IL-17 expression in WT and IKO CD4$^+$ T cells in Th17 conditions for 3d. Right: percentage of IL-17$^+$ cells among WT and IKO CD4$^+$ T cells, in Th17 conditions, in each division peak (n=4; mean ± SEM).

Fig. S11. Ikaros loss changes the landscape of chromatin accessibility in CD4$^+$ T cells.

(A) Seqminer heat map of all ATAC-seq peaks in WT and TKO CD4$^+$ T cells at d0 (67165 peaks) and at d1 of Th0 cultures (78378 peaks). **(C)** Pie chart of the genomic location distribution of all ATAC-seq peaks in WT and TKO CD4$^+$ T cells at d0 and d2 in Th0 cultures. **(B)** Volcano plot showing log_2FC TKO/WT identified by ATAC-seq in naïve T cells (d0) and in-vitro-differentiated T cells at day 2 (Th0 d2). Up- and down-regulated genes with changes significantly greater than Log_2FC ≥ 1 or ≤ -1 are highlighted in red and blue, respectively (padj ≤ 0.01). At d0, red dots: 3969 peaks; blue dots: 2740 peaks; in Th0 d2, red dots: 8950, blue dots: 6380. **(D)** Integration of RNA-seq data and ATAC-Seq data from TKO cells compared to WT cells at d0 and d1 of Th0 cultures. Left: In naive T cells at d0, only the 3677 peaks with a padj ≤ 0.05 in the ATAC-seq AND RNA-seq analysis are depicted. Among them, 1491 peaks have a log_2FC (TKO/WT) ≥ 1 or ≤ -1 with a Pearson correlation equal to 0.63 with a p value< 2.2^{-16}. Right: In the Th0 d1 condition, only the 9954 peaks with a padj ≤ 0.05 in the ATAC-seq and RNA-seq analysis are depicted. Among them, 2995 peaks have

a log2FC (TKO/WT) ≥ 1 or ≤ -1 in both analysis and have a Pearson correlation coefficient equal to 0.59 with a p value< 2.2^{-16}. Genes with a positive (purple) or a negative (black) correlation between ATAC-seq and RNA-seq data are highlighted. **(E)** Genome track view of ATAC-seq profiles of *Il3* (left) and *Ifng (right)* genes. The University of California Santa Cruz Genome browser (UCSC) depicts the pooled profile of the three independent experiments in in WT and TKO $CD4^+$ T cells at d0 and d1-2 in Th0 cultures.

Fig. S12. Ikaros loss leads to an enrichment of NFκB and Stat5 motifs on open chromatin regions.

(A) Heat map showing GO of the ATAC-seq peaks significantly increased (1219 peaks at d0 and 2687 peaks at Th0d1) and decreased (900 at d0 and 3040 at Th0 d1) in TKO compared to WT at d0 and d1 in Th0 cultures. Peaks are considered significantly increased in the TKO when the log_2FC (TKO/WT) > 2 with a padj ≤ 0.01, while they are considered significantly decreased in TKO when the log_2FC (TKO/WT) <- 2 with a padj ≤ 0.01. **(B)** Bar graph showing the indicated transcription factor motifs significantly enriched in WT and TKO ATAC-seq peaks at d0 (upper panel) and d1 in Th0 cultures (lower panel). The motifs were identified from AME-MEME motif search. Significant peaks were selected as in A.

Fig. S13. ChIP-seq analysis of Ikaros binding profile on differentially expressed genes.

(A) Pie chart of the genomic location distribution of all Ikaros peaks in WT naive $CD4^+$ T cells at d0 and at d1 in Th0 cultures. **(B)** UCSC Genome track views of ChIP-seq showing genes with a binding Ikaros on promoters or enhancers and genes not bound by Ikaros.

Table S1. Sequences of the primers used for RT-qPCR.

Table S2. Oligonucleotide probes used for EMSA.

SI REFERENCES

1. M. A. Medici, M. T. Sciortino, D. Perri, C. Amici, E. Avitabile, M. Ciotti, E. Balestrieri, E. De Smaele, G. Franzoso, A. Mastino, Protection by Herpes Simplex Virus Glycoprotein D against Fas-mediated Apoptosis, *J Biol Chem* **278**, 36059–36067 (2003).

2. L. Faletti, L. Peintner, S. Neumann, S. Sandler, T. Grabinger, S. Mac Nelly, I. Merfort, C.-H. Huang, D. Tschaharganeh, T.-W. Kang, F. Heinzmann, L. D'Artista, U. Maurer, T. Brunner, S. Lowe, L. Zender, C. Borner, TNFα sensitizes hepatocytes to FasL-induced apoptosis by NFκB-mediated Fas upregulation, *Cell Death and Disease* **9**, 909 (2018).

3. A. Lainé, B. Martin, M. Luka, L. Mir, C. Auffray, B. Lucas, G. Bismuth, C. Charvet, Foxo1 Is a T Cell-Intrinsic Inhibitor of the RORγt-Th17 Program, *The Journal of Immunology* **195**, 1791–1803 (2015).

4. E. Kleinmann, A.-S. Geimer Le Lay, M. Sellars, P. Kastner, S. Chan, Ikaros represses the transcriptional response to Notch signaling in T-cell development, *Mol Cell Biol* **28**, 7465–7475 (2008).

5. C. Charvet, A. J. Canonigo, S. Bécart, U. Maurer, A. V. Miletic, W. Swat, M. Deckert, A. Altman, Vav1 promotes T cell cycle progression by linking TCR/CD28 costimulation to FOXO1 and p27kip1 expression, *J Immunol* **177**, 5024–5031 (2006).

6. D. Dembele, P. Kastner, Fold change rank ordering statistics: a new method for detecting differentially expressed genes, *BMC Bioinformatics* **15** (2014), doi:10.1186/1471-2105-15-14.

7. Y. Zheng, S. Z. Josefowicz, A. Kas, T.-T. Chu, M. A. Gavin, A. Y. Rudensky, Genome-wide analysis of Foxp3 target genes in developing and mature regulatory T cells, *Nature* **445**, 936–940 (2007).

8. A. Oravecz, A. Apostolov, K. Polak, B. Jost, S. Le Gras, S. Chan, P. Kastner, Ikaros mediates gene silencing in T cells through Polycomb repressive complex 2, *Nature Communications* **6**, 1–15 (2015).

9. B. Langmead, C. Trapnell, M. Pop, S. L. Salzberg, Ultrafast and memory-efficient alignment of short DNA sequences to the human genome, *Genome Biology* **10**, R25 (2009).

10. Y. Zhang, T. Liu, C. A. Meyer, J. Eeckhoute, D. S. Johnson, B. E. Bernstein, C. Nusbaum, R. M. Myers, M. Brown, W. Li, X. S. Liu, Model-based analysis of ChIP-Seq (MACS), *Genome Biology* **9**, R137 (2008).

11. S. Heinz, C. Benner, N. Spann, E. Bertolino, Y. C. Lin, P. Laslo, J. X. Cheng, C. Murre, H. Singh, C. K. Glass, Simple Combinations of Lineage-Determining Transcription Factors Prime cis-Regulatory Elements Required for Macrophage and B Cell Identities, *Mol Cell* **38**, 576–589 (2010).

12. W. J. Kent, C. W. Sugnet, T. S. Furey, K. M. Roskin, T. H. Pringle, A. M. Zahler, D. Haussler, The human genome browser at UCSC, *Genome Res.* **12**, 996–1006 (2002).

13. T. Ye, A. R. Krebs, M.-A. Choukrallah, C. Keime, F. Plewniak, I. Davidson, L. Tora, seqMINER: an integrated ChIP-seq data interpretation platform, *Nucleic Acids Res* **39**, e35–e35 (2010).

14. M. I. Love, W. Huber, S. Anders, Moderated estimation of fold change and dispersion for RNA-seq data with DESeq2, *Genome Biology* **15**, 1–21 (2014).

15. R. C. McLeay, T. L. Bailey, Motif Enrichment Analysis: a unified framework and an evaluation on ChIP data, *BMC Bioinformatics* **11**, 1–11 (2010).

16. A. Subramanian, P. Tamayo, V. K. Mootha, S. Mukherjee, B. L. Ebert, M. A. Gillette, A. Paulovich, S. L. Pomeroy, T. R. Golub, E. S. Lander, J. P. Mesirov, Gene set enrichment analysis: A knowledge-based approach for interpreting genome-wide expression profiles, *Proc Natl Acad Sci USA* **102**, 15545–15550 (2005).

17. A. Liberzon, C. Birger, H. Thorvaldsdóttir, M. Ghandi, J. P. Mesirov, P. Tamayo, The Molecular Signatures Database Hallmark Gene Set Collection, *Cell Systems* **1**, 417–425 (2015).

18. T. Galili, A. O'Callaghan, J. Sidi, C. Sievert, J. Wren, Ed. heatmaply: an R package for creating interactive cluster heatmaps for online publishing, *BMC Bioinformatics* **34**, 1600–1602 (2018).

19. M. Martin, Cutadapt removes adapter sequences from high-throughput sequencing reads, *EMBnet j.* **17**, 10 (2011).

20. A. Dobin, C. A. Davis, F. Schlesinger, J. Drenkow, C. Zaleski, S. Jha, P. Batut, M. Chaisson, T. R. Gingeras, STAR: ultrafast universal RNA-seq aligner, *Bioinformatics* **29**, 15–21 (2012).

21. S. Anders, P. T. Pyl, W. Huber, HTSeq--a Python framework to work with high-throughput sequencing data, *Bioinformatics* **31**, 166–169 (2015).

22. S. Anders, W. Huber, Differential expression analysis for sequence count data, *Genome Biology* **11**, R106 (2010).

23. Y. Zhou, Bin Zhou, L. Pache, M. Chang, A. H. Khodabakhshi, O. Tanaseichuk, C. Benner, S. K. Chanda, Metascape provides a biologist-oriented resource for the analysis of systems-level datasets, *Nature Communications*, 1–10 (2019).

24. Y. Lee, A. Awasthi, N. Yosef, F. J. Quintana, S. Xiao, A. Peters, C. Wu, M. Kleinewietfeld, S. Kunder, D. A. Hafler, R. A. Sobel, A. Regev, V. K. Kuchroo, Induction and molecular signature of pathogenic TH17 cells, *Nat Immunol* **13**, 991–999 (2012).

25. W. Sheng, F. Yang, Y. Zhou, H. Yang, P. Y. Low, D. M. Kemeny, P. Tan, A. Moh, M. H. Kaplan, Y. Zhang, X.-Y. Fu, STAT5 programs a distinct subset of GM-CSF-producing T helper cells that is essential for autoimmune neuroinflammation, *Cell Res* **24**, 1387–1402 (2014).

26. R. Qiu, X. Yu, L. Wang, Z. Han, C. Yao, Y. Cui, G. Hou, D. Dai, W. Jin, N. Shen, Inhibition of Glycolysis in Pathogenic TH17 Cells through Targeting a miR-21-Peli1-c-Rel Pathway Prevents Autoimmunity, *The Journal of Immunology* **204**, 3160–3170 (2020).

Supplemental Figure 1

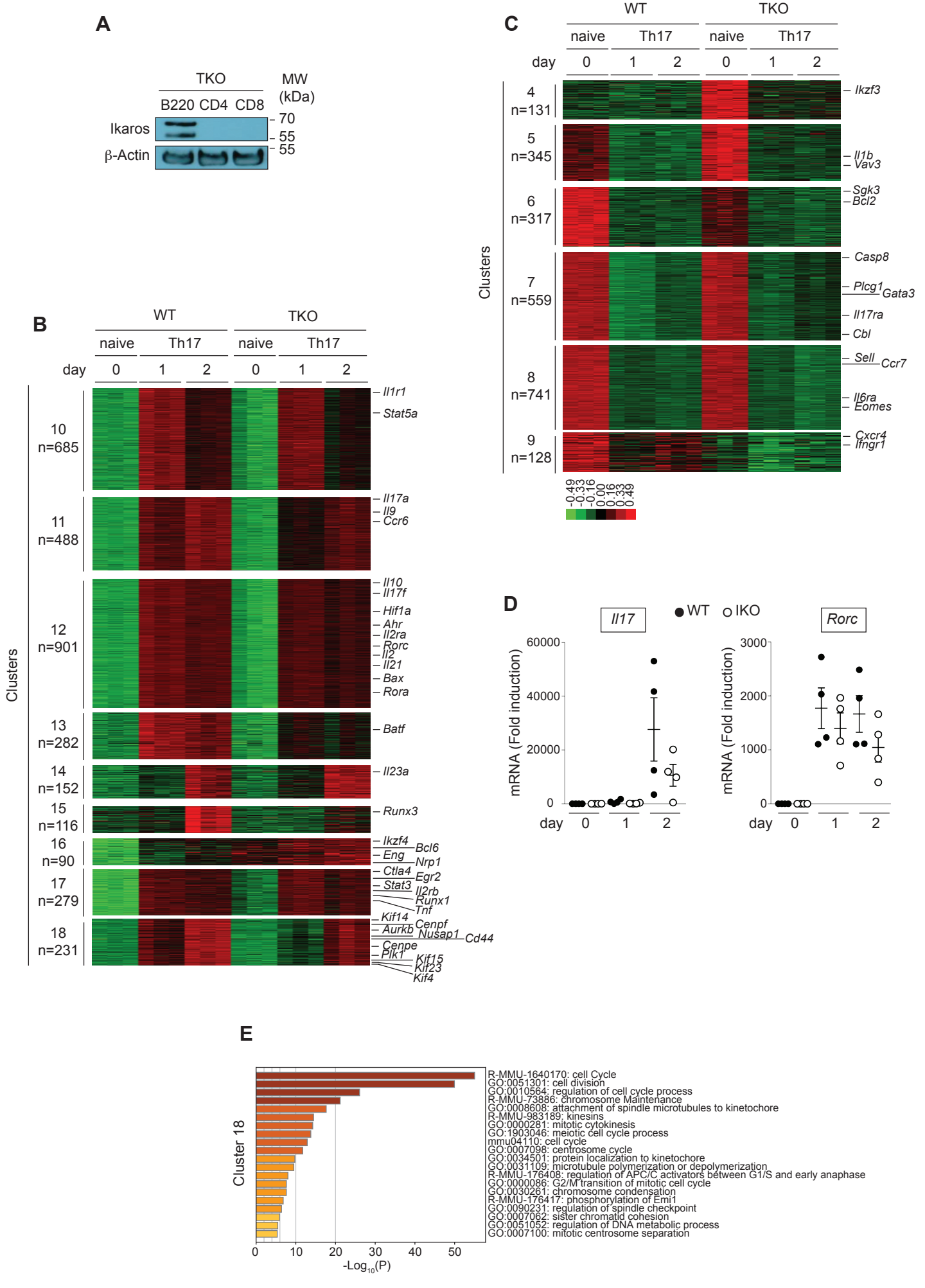

Supplemental Figure 2

A

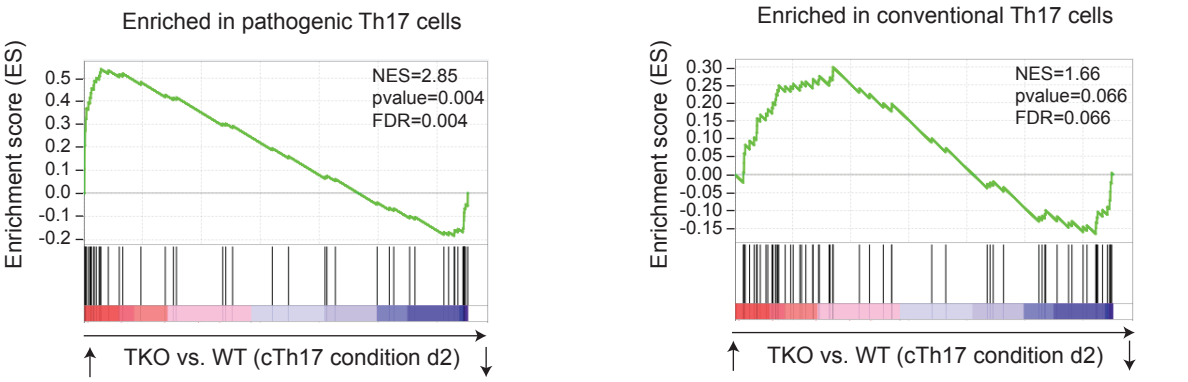

B

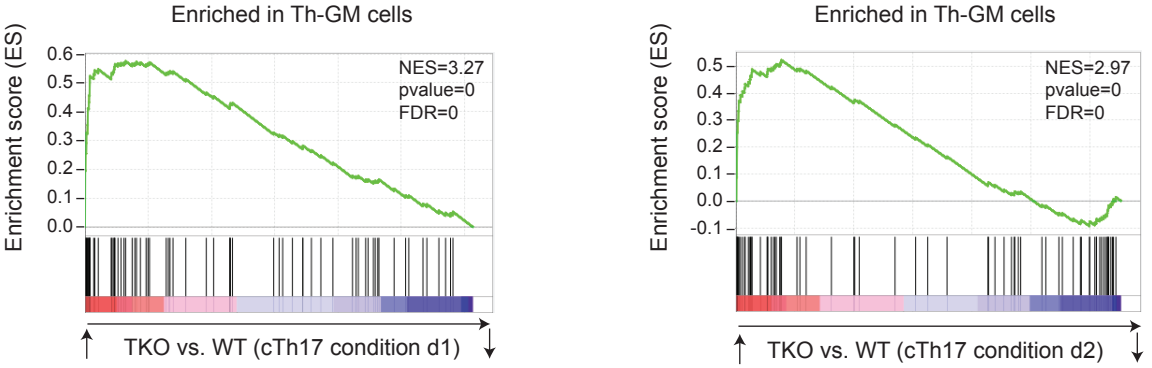

C

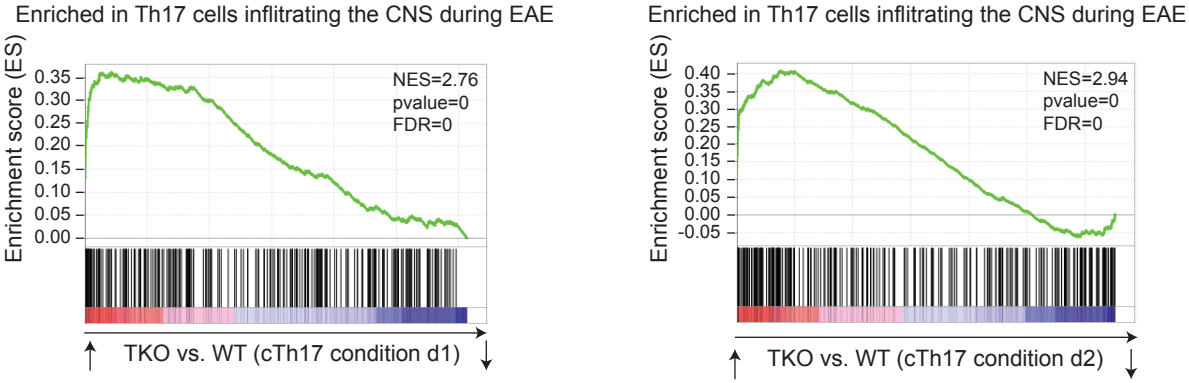

Supplemental Figure 3

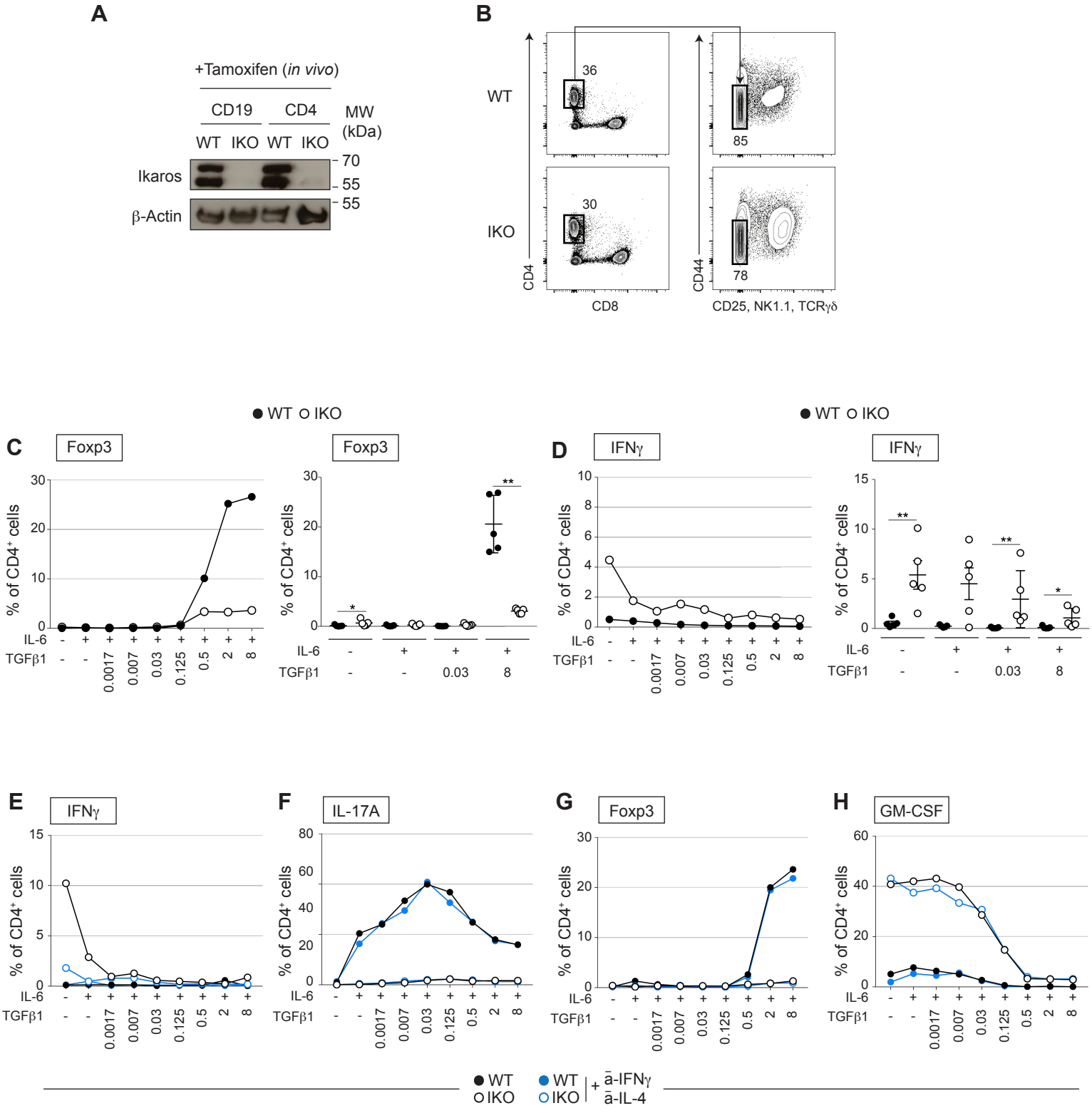

Supplemental Figure 4

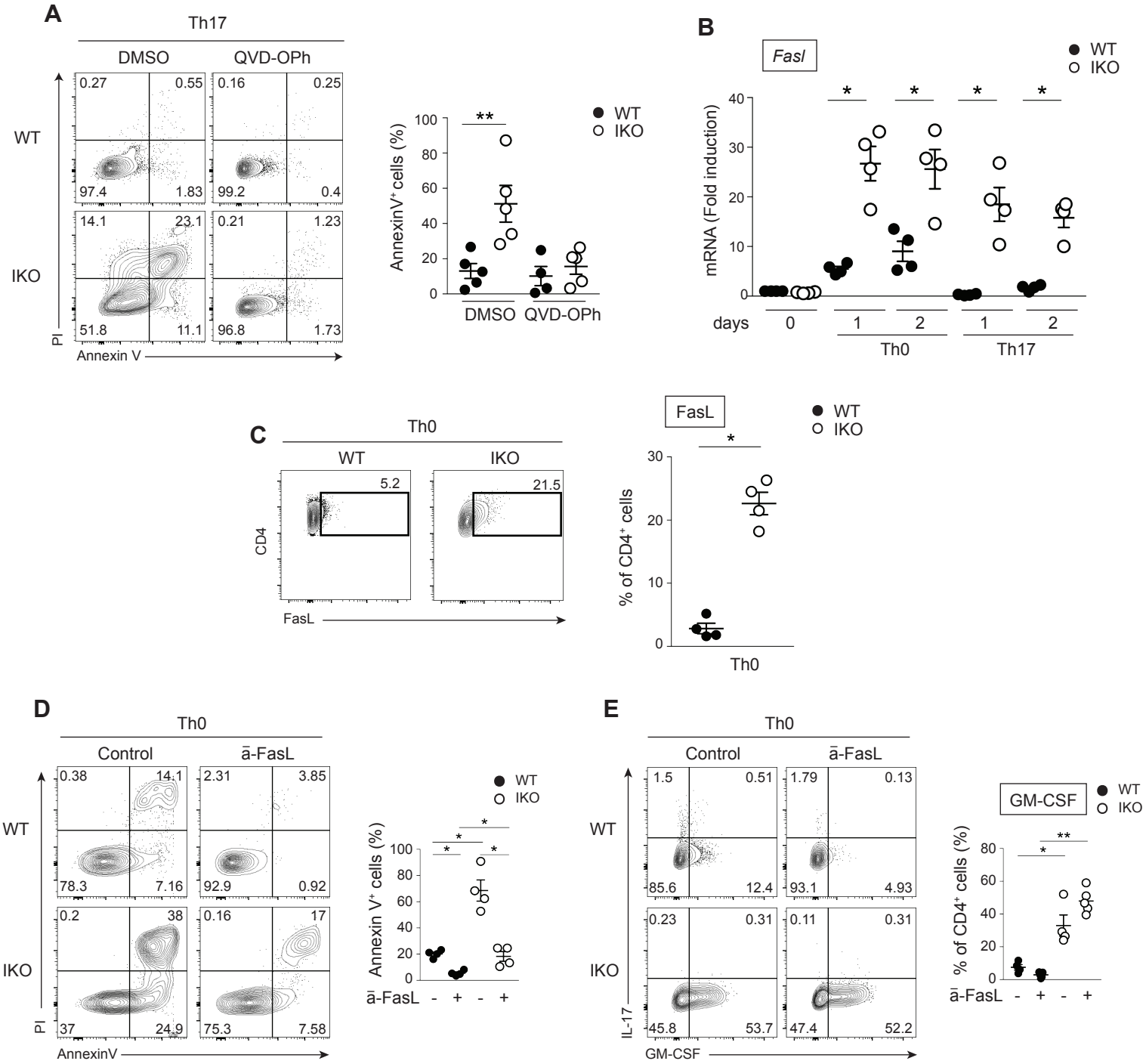

Supplemental figure 5

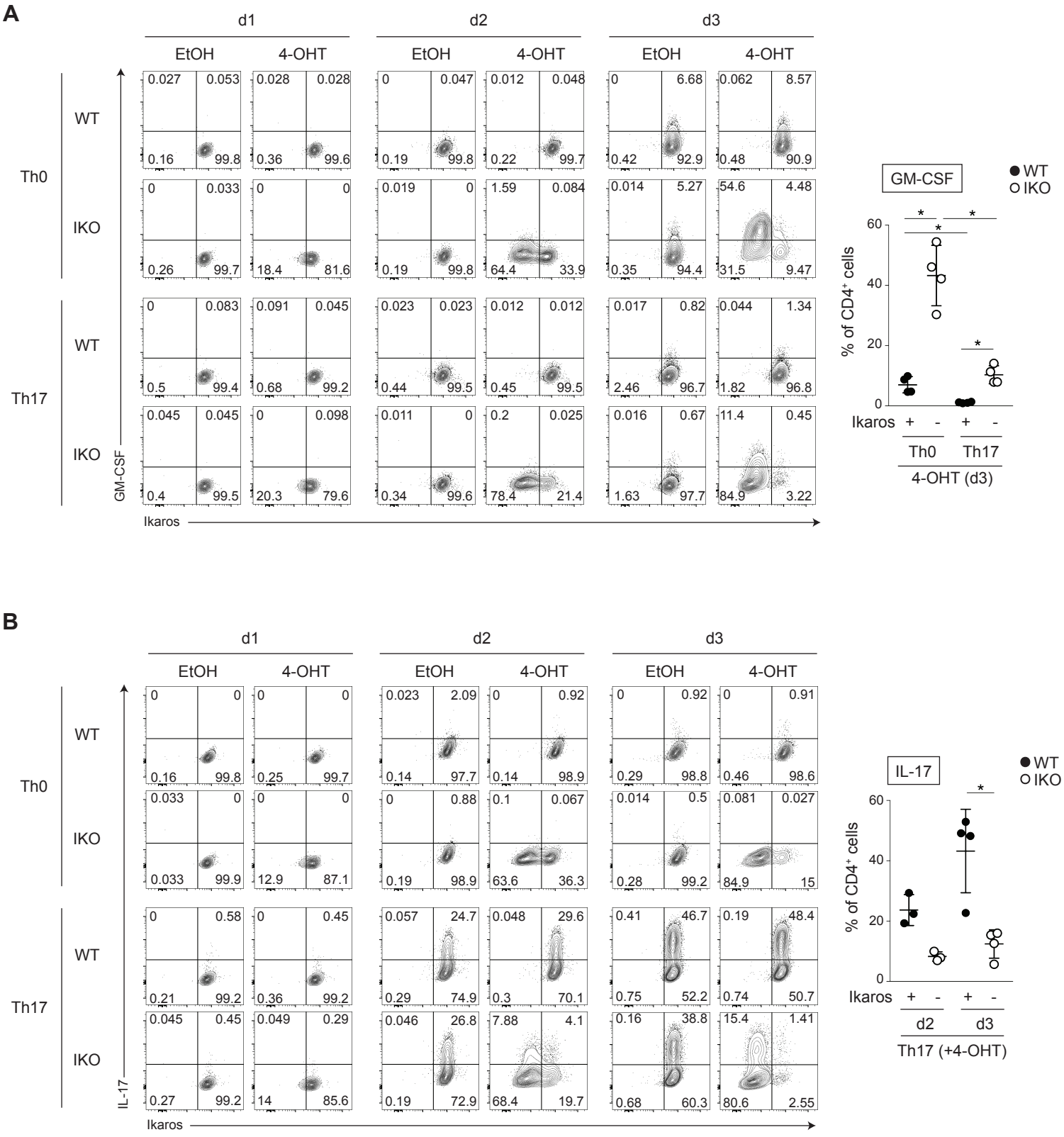

Supplemental Figure 6

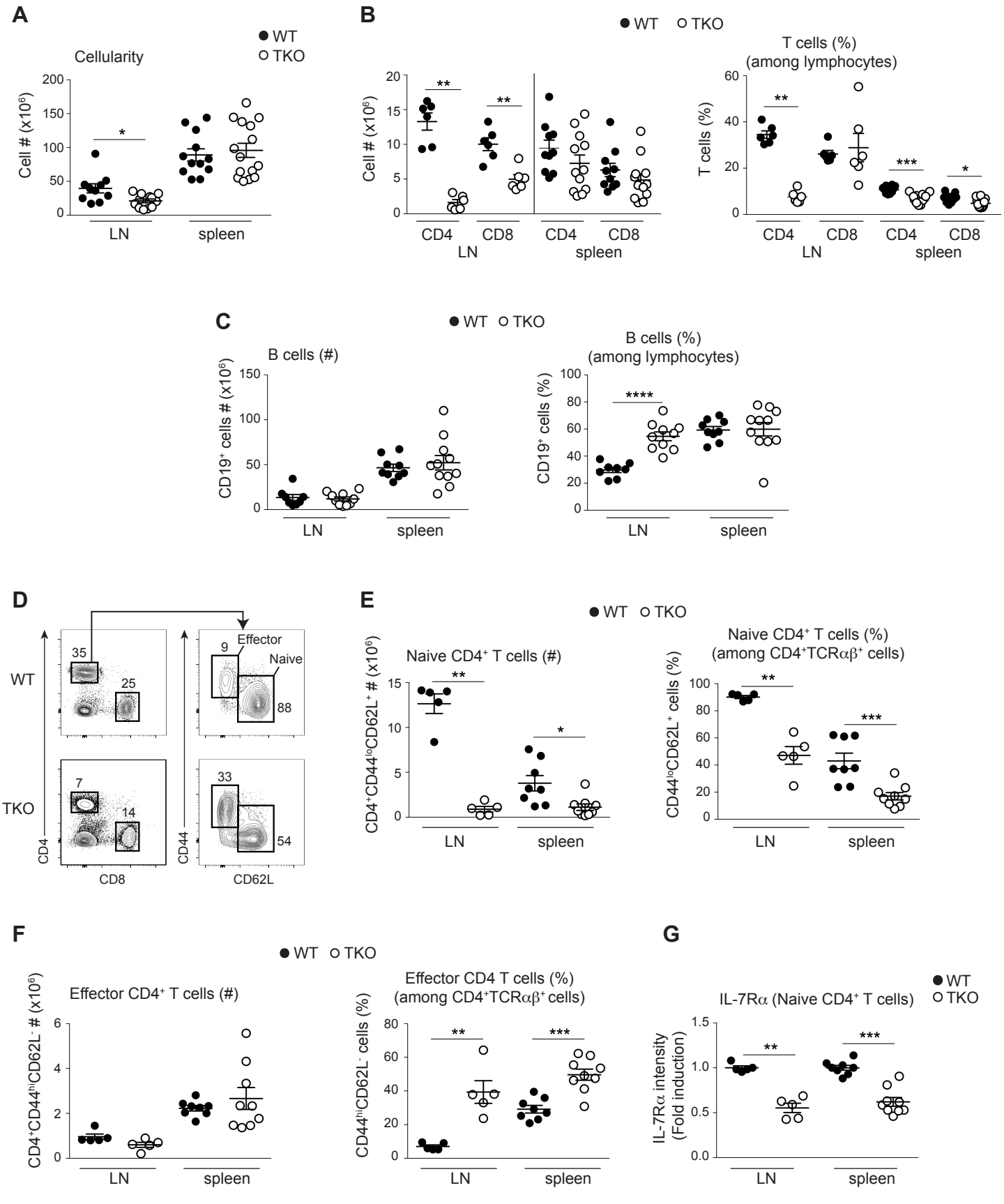

Supplemental Figure 7

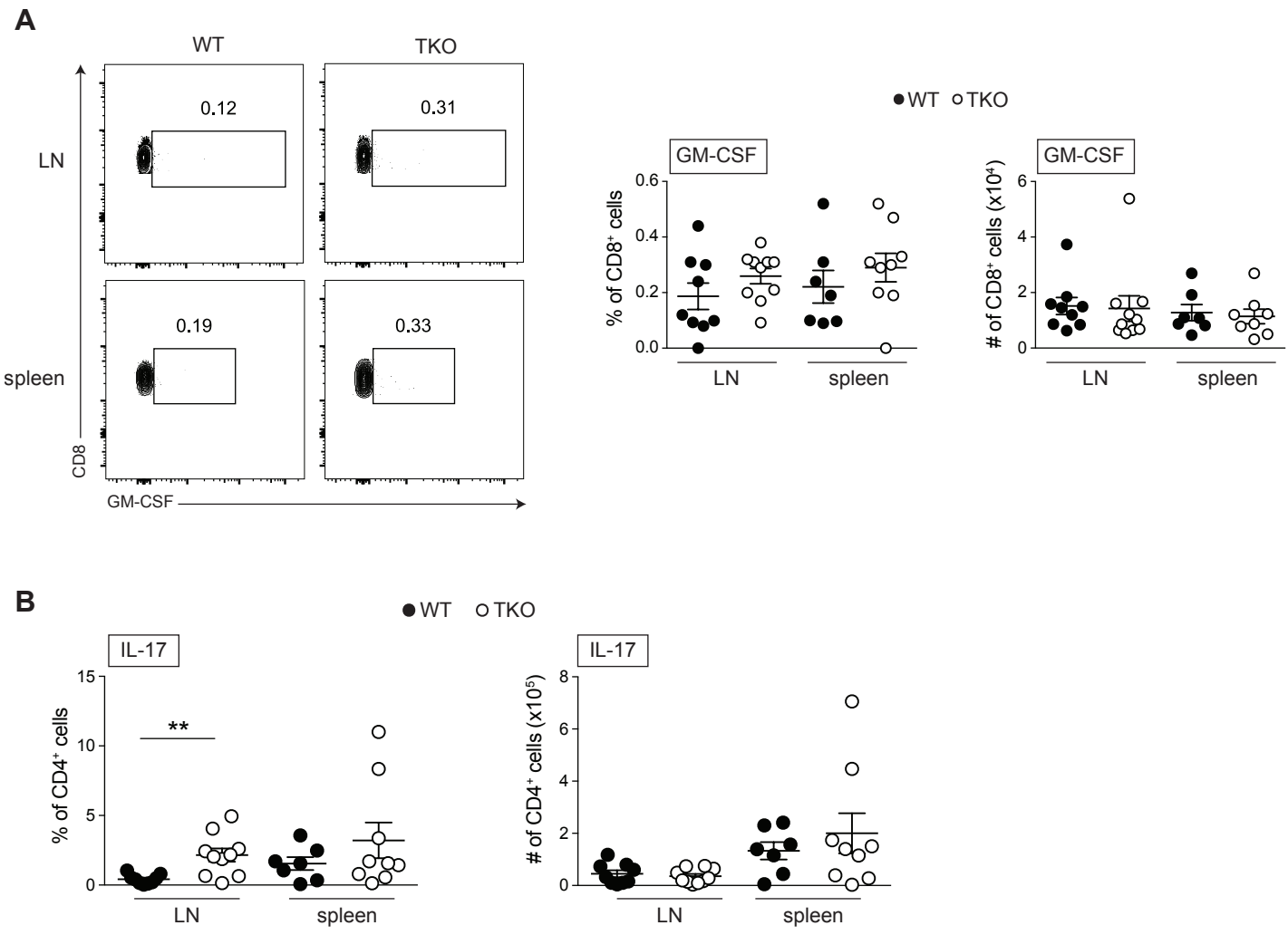

Supplemental Figure 8

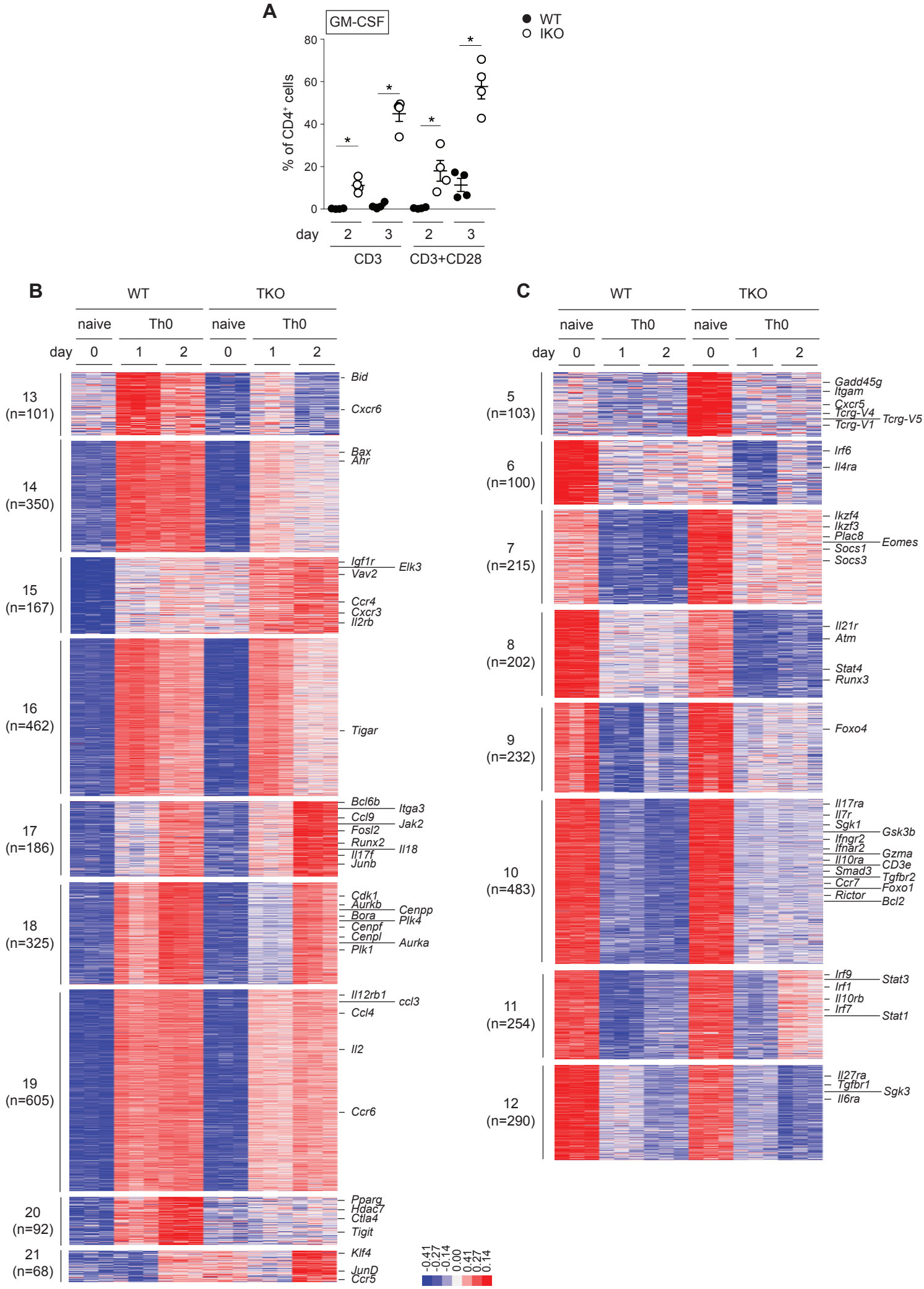

Supplemental Figure 9

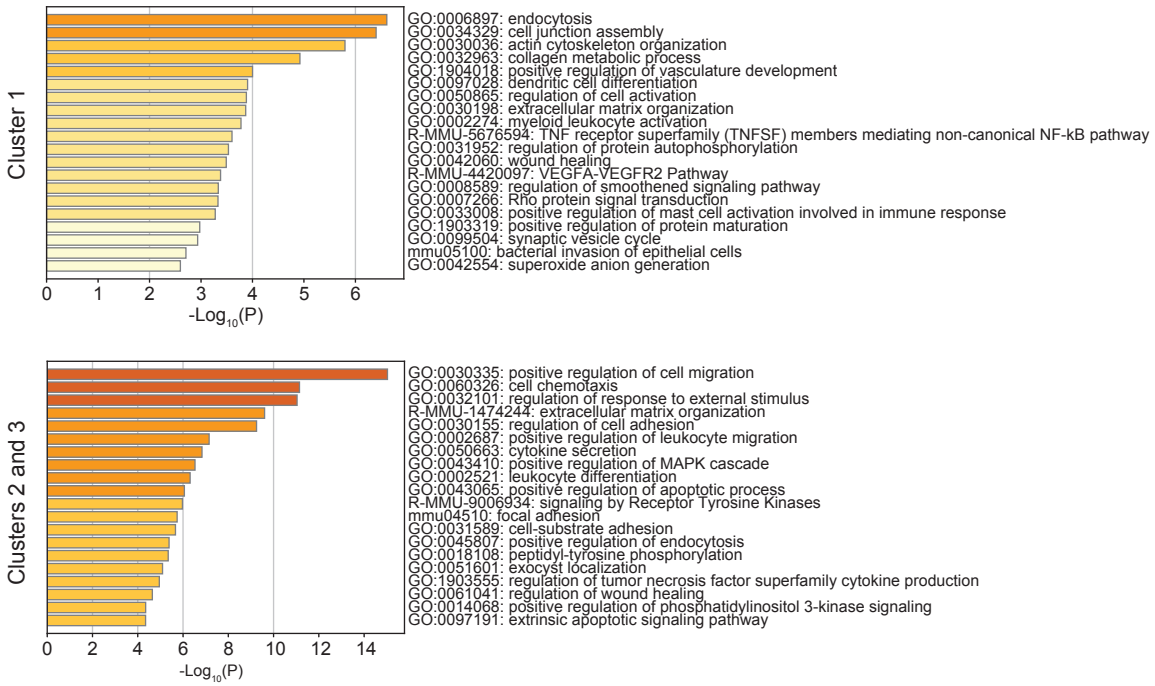

Supplemental Figure 10

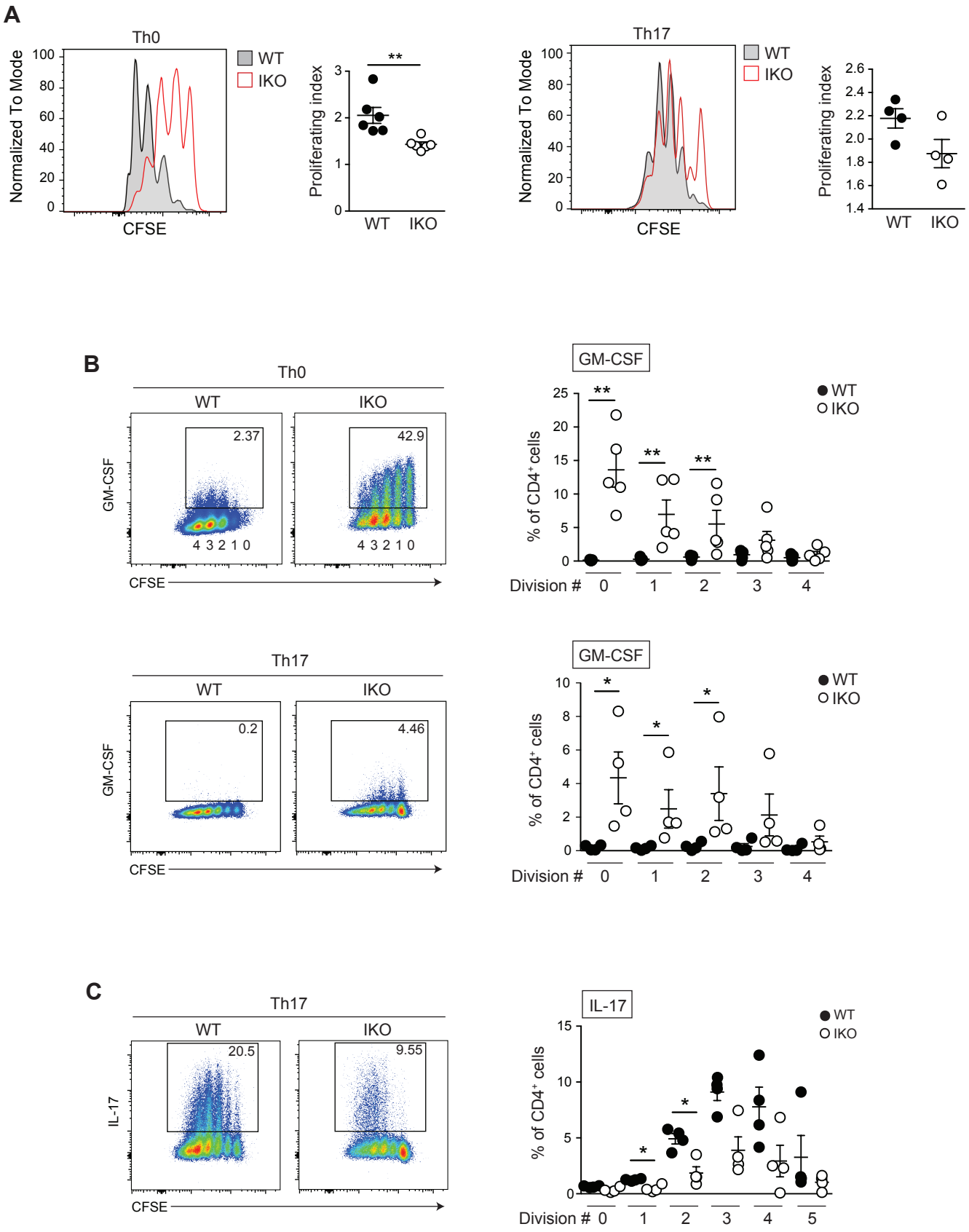

Supplemental Figure 11

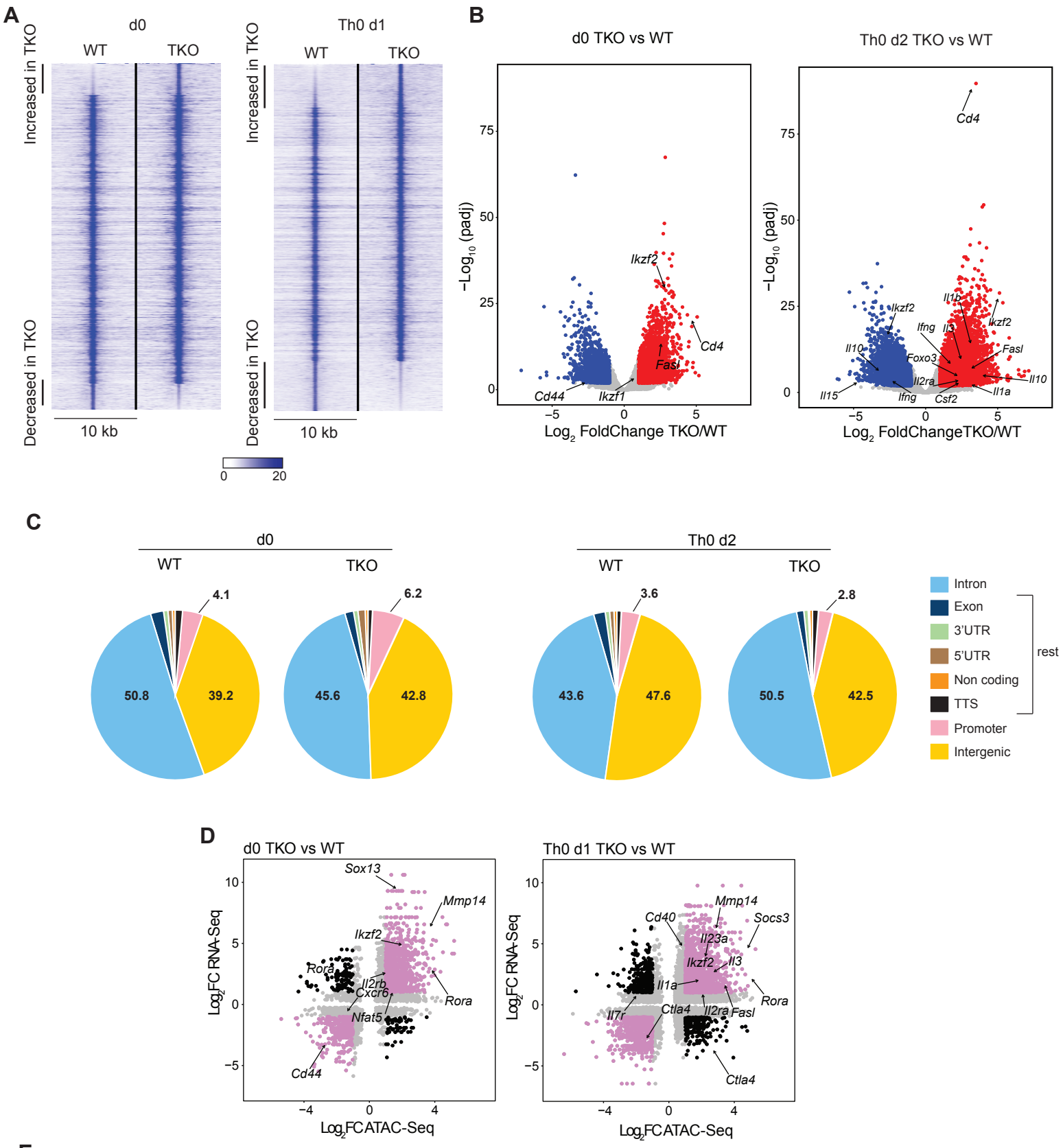

Supplemental Figure 12

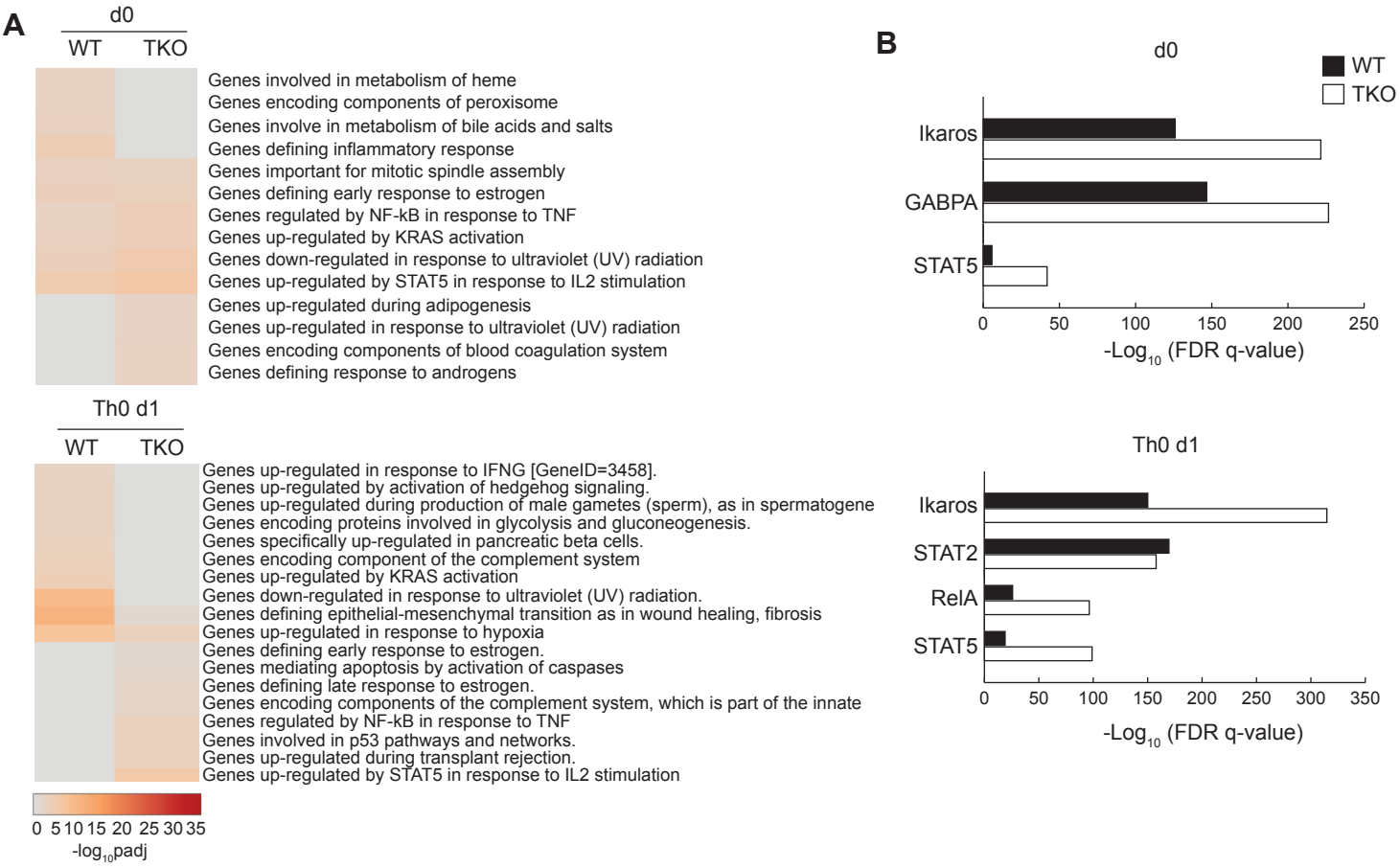

Supplemental Figure 13

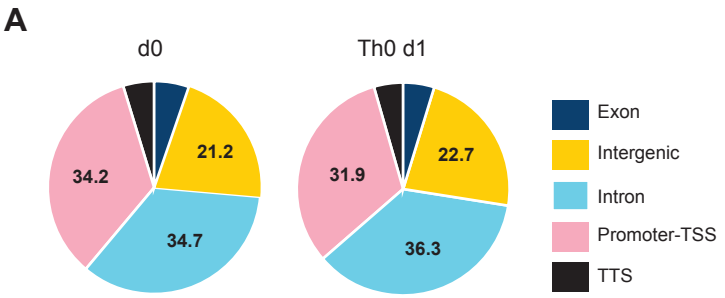

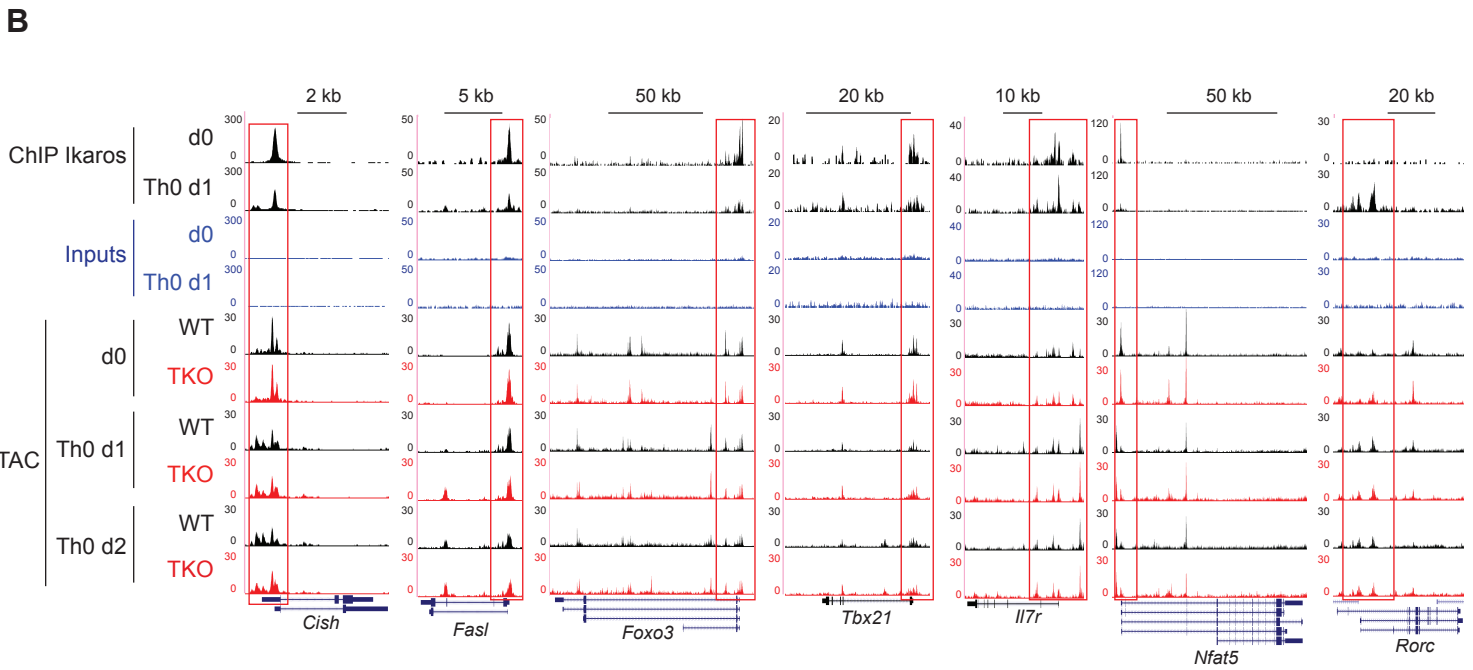

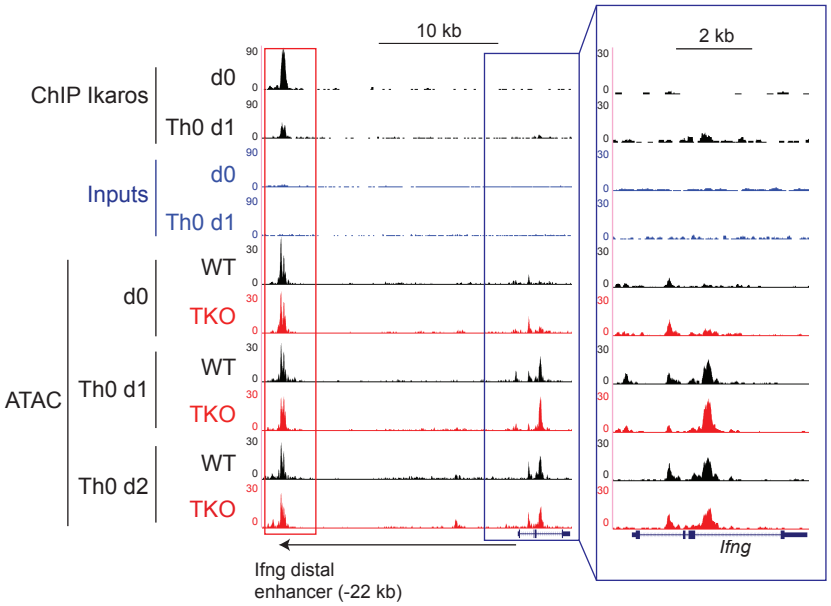

Supplemental Table 1

Name	Primer sequence (5'-3')
m*Csf2* F	TCGTCTCTAACGAGTTCTCCTT
m*Csf2* R	CGTAGACCCTGCTCGAATATCT
m*Ifng* F	CGGCACAGTCATTGAAAGCC
m*Ifng* R	TGTCACCATCCTTTTGCCAGT
m*Il3* F	ATAGGGAAGCTCCCAGAACCT
m*Il3* R	GGATCCACTTCTCCTTGGCT
m*Fasl* F	TTCACCAACCAAAGCCTTAAAG
m*Fasl* R	GCTGGTTGTTGCAAGACTGA
m*RORc* F	TCACCTGTGAGGGGTGCAAG
m*RORc* R	GTTCGGTCAATGGGGCAGTT
m*Il17* F	ATCCCTCAAAGCTCAGCGTGTC
m*Il17* R	GGGTCTTCATTGCGGTGGAGAG
m*L32* F	TTAAGCGAAACTGGCGGAAAC
m*L32* R	TTGTTGCTCCCATAACCGATG
m*Il10* F	CAGTACAGCCGGGAAGACAA
m*Il10* R	TGGCAACCCAAGTAACCCTTA
h*CSF2* F	GCGTCTCCTGAACCTGAGTA
h*CSF2* R	GTGCTGCTTGTAGTGGCTG
h*L32* F	AGGCATTGACAACAGGGTTC
h*L32* R	GTTGCACATCAGCAGCACTT

Supplemental Table 2

Name	Probe sequence (5'-3')
site 1	GGTTTCTGTAACAGGAAGTGATTTA
site 2	GATATGGGGTTTTCAAAGAATGTTT
site 3	AAAGGATGGGCAATTTCCCACTGTC
site 4	GTCTCTCTGGTGGAAAGCGAAGCTG
sites 5+6	GTTTTCCCTGGATTCCGAGCTGCCT
sites 5+6 (mut 5)	GTTTGACCTGGATTCCGAGCTGCCT
sites 5+6 (mut 6)	GTTTTCCCTGGATGACGAGCTGCCT
sites 5+6 (mut 5+6)	GTTTGACCTGGATGACGAGCTGCCT
sites 4+5+6	GTCTCTCTGGTGGAAAGCGAAGCTGGTTTTCCCTGGATTCCGAGCTGCCT
sites 4+5+6 (mut 4)	GTCTCTCTGGTGTCAAGCGAAGCTGGTTTTCCCTGGATTCCGAGCTGCCT
sites 4+5+6 (mut 5+6)	GTCTCTCTGGTGGAAAGCGAAGCTGGTTTGACCTGGATGACGAGCTGCCT
BS4	TCAGCTTTTGGGAATGTATTCCCTGTCA
Cish	CCAGTTTTCCTGGAAAGTTCTTGGAAATCT